

Article

Current-Based Coordination of Distributed Energy Resources in a Grid-Connected Low-Voltage Microgrid: An Experimental Validation of Adverse Operational Scenarios

Augusto M. S. Alonso ^{1,*}, Luis De Oro Arenas ², Danilo I. Brandao ³, Elisabetta Tedeschi ^{4,5},
Ricardo Q. Machado ¹ and Fernando P. Marafão ²

¹ Department of Electrical and Computer Engineering, University of São Paulo, São Carlos 13566-590, SP, Brazil

² Group of Automation and Integrated Systems, São Paulo State University, Sorocaba 18087-180, SP, Brazil

³ Graduate Program in Electrical Engineering, Universidade Federal de Minas Gerais, Belo Horizonte 31270-901, MG, Brazil

⁴ Department of Electric Power Engineering, Norwegian University of Science and Technology, 7491 Trondheim, Norway

⁵ Department of Industrial Engineering, University of Trento, Povo, 38123 Trento, Italy

* Correspondence: augusto.alonso@usp.br

Abstract: Low-voltage grid-connected microgrids rely on the exploitation of inverter-interfaced distributed energy resources (DERs) in order to feed loads and to achieve bidirectional power flow controllability at their point of common coupling (PCC) with the upstream grid. However, adverse operational conditions, such as the existence of DERs of different operation natures, DERs of non-equal power ratings, as well as the occurrence of non-steady and non-sinusoidal grid voltage scenarios, bring complications to microgrid energy management. Consequently, control strategies employed to coordinate DERs in dispatchable microgrids need to be resilient to such non-ideal conditions. Hence, this paper demonstrates that a multi-purpose strategy, so-called the Generalized Current-Based Control (GCBC) approach, is capable of steering DERs under such adverse operational scenarios, ensuring proportional current sharing among them while also regulating the microgrid power dispatchability at the PCC. The discussions are supported by an extensive experimental validation on a laboratory-scale single-phase microgrid prototype, demonstrating that the GCBC approach allows DERs of different operational natures to be coordinated, respecting their power ratings, and allowing the single-controllable microgrid to endure operation under distorted voltages and support voltage ride-through conditions.

Keywords: current sharing; dispatchable microgrid; distorted voltages; distributed energy resources; inverters; power quality; voltage ride through



Citation: Alonso, A.M.S.; Arenas, L.D.O.; Brandao, D.I.; Tedeschi, E.; Machado, R.Q.; Marafão, F.P. Current-Based Coordination of Distributed Energy Resources in a Grid-Connected Low-Voltage Microgrid: An Experimental Validation of Adverse Operational Scenarios. *Energies* **2022**, *15*, 6407. <https://doi.org/10.3390/en15176407>

Academic Editor: Emilio Lorenzani

Received: 27 July 2022

Accepted: 22 August 2022

Published: 2 September 2022

Publisher's Note: MDPI stays neutral with regard to jurisdictional claims in published maps and institutional affiliations.



Copyright: © 2022 by the authors. Licensee MDPI, Basel, Switzerland. This article is an open access article distributed under the terms and conditions of the Creative Commons Attribution (CC BY) license (<https://creativecommons.org/licenses/by/4.0/>).

1. Introduction

Small-scale distributed energy resources (DERs) have spread fast over AC low-voltage (LV) electrical power grids [1,2], becoming key players in the actual clean energy transition sought worldwide, particularly due to their capability of incorporating renewable energy sources (RESs) and energy storage systems (ESSs) into their physical structure [3,4]. In general, DERs also take advantage of power electronic inverters as interface elements with the grid, allowing them not only to provide active power conversion from the energy source at their DC side but also to offer multiple ancillary services [5–7] at their AC side. Among the numerous complementary functionalities offered by such DERs, the grid-support and power quality-related services (e.g., reactive power control, harmonic compensation, voltage regulation, and so forth) are among the most promising ones for the present and near future of LV grids [5,8,9].

An interesting scenario in which such ancillary services' provision is highly appreciated is the one of LV microgrids (MGs) [10–13], which are electrical systems dominated by

DERs and composed of a considerable amount of linear and non-linear loads. Moreover, as seen in Figure 1, MGs present other particularities of operation that have motivated a considerable amount of research in the past decades [12,14–16]: (i) their flexibility to be controlled as a single entity with respect to the point of common coupling (PCC) with the upstream LV grid (i.e., as a dispatchable entity [17,18]) and (ii) their ability to operate either interconnected or islanded [19,20]. Nevertheless, as a consequence of the MGs' multiple management features, coordinated control strategies need to be implemented to adequately exploit DERs to support a controlled power dispatchability at the MG PCC, as well to achieve power quality interventions [13,21].

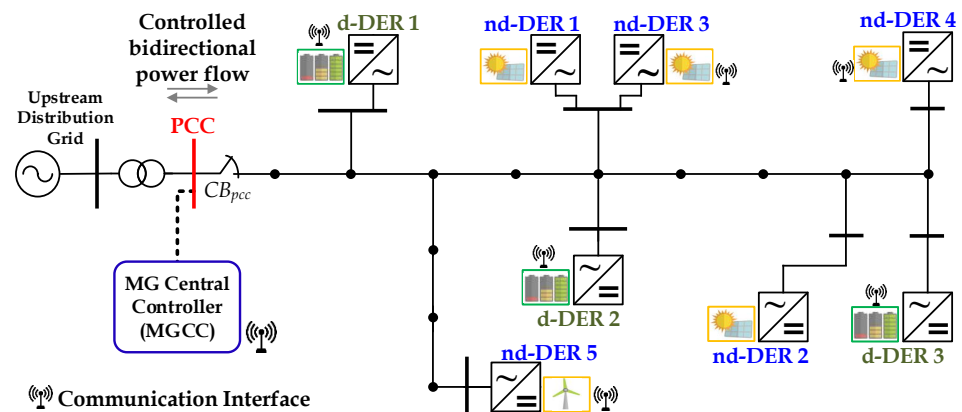


Figure 1. Example of a dispatchable MG interconnected to an upstream grid, comprising multiple DERs of assorted natures and different operational conditions, being managed by an MGCC.

The demand for flexible, coordinated control strategies is particularly justified by the MGs' diversity of apparatuses [10], because they usually need to manage DERs of assorted operational natures, such as dispatchable (d-DERs) (e.g., the ones based on ESSs) and non-dispatchable elements (nd-DERs) (e.g., pv-based and wind-based systems, etc.) [20]. Additionally, such electrical systems present other inherent operational complications caused by the existence of DERs of non-equal power ratings, which leads to non-proportional power sharing within the MG, besides the fact that remote control capabilities might not always be available for all DERs, forcing coordination strategies to cope with this perspective. Other common concerns to be taken into account are those related to voltage quality, because LV MGs likely face non-sinusoidal or non-steady voltages conditions over time [22,23], consequently bringing additional energy management and stability challenges.

In the literature, several previous papers have proposed coordination strategies for DERs within the MG perspective, considering the above-mentioned adverse operational conditions. For instance, refs. [24–26] presented control approaches focused on the implementation of droop-controlled DERs to achieve better power quality indexes and proportional power sharing. Similarly, by using adaptations in droop-based control functions and based on the implementation of virtual impedance loops, refs. [27–29] presented strategies to achieve accurate active and reactive power sharing among the DERs in MGs. In [20,30], the challenge of having DERs of different operational natures is addressed. For the former approach, it is demonstrated that the AC bus-signaling strategy allows to obtain satisfactory energy management for the MG, and for the latter strategy, a hierarchical topology supports the coordination of the DERs. Nonetheless, for all these previous strategies, as well as for many others found in the literature [31–33], focus is given to the islanded mode of operation, not addressing the mutual concern for controlling the MG power dispatchability to support an upstream grid.

On the other hand, the coordination of DERs in grid-connected MGs is less discussed in the literature, although a considerable amount of research has already been performed. For instance, refs. [34–37] discuss how inverters can be adequately steered in LV MGs while considering the interconnection to an upstream grid. Focus is given to the implementation

of a centralized controller that exchanges control data with the inverters (i.e., similarly to Figure 1), using low-bandwidth communication channels as the means to set control setpoints for the coordination. As a result, such papers demonstrate that proper power sharing and control over the power dispatchability to the upstream grid can be attained. Considerations for accommodating multiple DERs and achieving energy management in dispatchable LV MGs are also presented in [38,39]. Moreover, the controllability over the MG power flow is discussed thoroughly in [17,18,40,41], reinforcing the importance of managing such an operational functionality. Yet, the literature shows that the controllability at the interconnection point with the upstream grid (i.e., the PCC) can even support LV MGs to evolve to the E-LAN concept [42], allowing to achieve independent control of the currents in each feeder of the grid.

Another coordinated control methodology is extensively discussed in [43–45], being applied to the perspective of grid-connected MGs in which the active, reactive, and harmonic powers need to be shared among DERs. In such a case, the so-called Generalized Current-Based Control (GCBC) strategy is considered, having grounds on the remote control topology depicted in Figure 1. The GCBC relies on the central controller (MGCC) and on the analysis of current terms to coordinate DERs to support a multi-purpose MG operation. Consequently, active, reactive, and selective harmonic currents can be shared among the DERs proportionally to their nominal capabilities while also taking into consideration the regulation of the MG power flow at the PCC.

Nevertheless, although extensive explanations about the GCBC strategy have been provided in [43,44], and comparative studies against the state-of-the-art control approaches were carried out in [44,45], the existence of DERs of assorted natures (i.e., d-DER and nd-DERs) in the MG has not been explored yet. In addition, discussions and experimental validations have not been found in the literature for what concerns the GCBC's resilience of operation under adverse MG operational scenarios, such as non-ideal voltage conditions. Thus, this gap in the discussions in relation to such a strategy is the motivation for this paper. Lastly, it is worth mentioning that the flexibility of operation and the capability to withstand the coordination of DERs under non-ideal scenarios put the GCBC as a powerful alternative to achieve more reliable LV distribution systems. Consequently, the authors believe that the strategy will soon be seen by distribution system operators (DSOs) as a promising tool to manage DERs in real applications.

Paper Contributions and Organization

Taking into account the scenario of a grid-connected single-phase LV MG comprising multiple DERs being coordinated by a centralized entity, the contributions of this paper are three-fold, being given as follows:

- A duly detailed mathematical presentation of the GCBC strategy, demonstrating how such a control methodology steers DERs and manages the MG's power dispatchability at the PCC under several scenarios;
- Validation by means of experimental results that the GCBC allows to manage the MG considering the co-existence of d-DERs and nd-DERs. It is demonstrated that an adequate MG operation is also achieved in the presence of DERs without remote control interfaces. Moreover, the results show that proportional current sharing can be guaranteed among all DERs controlled by the GCBC;
- The experimental validation of the MG operation under non-sinusoidal and non-steady voltage conditions. Thus, it is demonstrated that the DERs controlled by the GCBC can endure operation when the grid suffers from distorted voltages, as well as when voltage ride-through resiliency is required.

This paper is organized as follows. In Section 2, the MG topology and control principles are presented to explain the context of the operation of the GCBC strategy and how it allows to obtain a coordinated operation of DERs. In Section 3, the laboratory prototype of the single-phase dispatchable MG is discussed and some preliminary operation results are presented. In Section 4, the experimental results of the MG operation upon adverse

scenarios are presented, highlighting the features of the GCBC strategy. Finally, Section 5 closes the paper with the conclusions of the research. It is finally highlighted that the term “adverse operational conditions” used in this paper focuses on the following concerns: (i) the existence of DERs of different operation natures; (ii) having DERs of non-equal power ratings; (iii) the occurrence of non-steady voltage profiles; and (iv) the unintentional imposition of non-sinusoidal voltages in the MG PCC by the upstream grid.

2. Microgrid and DER Control Principles

The motivation of the GCBC strategy rises from the challenges behind the mutual implementation of: (i) coordination algorithms to achieve current sharing among DERs in an LV MG and (ii) the desire to control a grid-connected MG as a single controllable entity (i.e., seen by the upstream grid perspective). Hence, to explain how the GCBC strategy operates, it is first required to discuss its main application scenario, leading to the discussions about the MG topology and control principles. The infrastructure of the considered LV MG scenario is presented in Figure 1, in which three main aspects need to be clarified.

The first aspect relates to the existence of a single PCC interconnecting the MG with an upstream grid, which is usually characterized by the placement of a distribution system transformer (DST). The PCC is an important branch of the electric circuit because it is where the MG power dispatchability is regulated, being also where the MGCC is preferably physically placed. The second aspect takes into account the LV scenario of application, which is typically characterized by having line impedances of a low X/R ratio (i.e., $X/R < 1.0$). Consequently, the cables impedances are predominantly resistive, which is an important consideration for the GCBC formulation, as explained in Section 2.1. The last aspect relates to the homogeneity of the MG elements, indicating that (i) line impedances present a similar impedance value per length at each branch of the circuit and that (ii) the DERs and loads are uniformly distributed throughout the MG and they present a fairly similar range of power density.

With regard to the control DERs, this paper considers that both d-DERs and nd-DERs exist in the MG. In addition, to cope with realistic scenarios, it is considered that remote control capability is not present for all DERs. Different types of control functionalities are considered for the DERs, according to the summary presented in Table 1. Note that the GCBC can only coordinate d-DERs and Type B nd-DERs. Particularly for the latter, control occurs only over their ancillary service provision (i.e., reactive and harmonic control) when they present the remaining power capability (i.e., due to their non-coordinated active power injections). Type A nd-DERs are not controlled by the GCBC because they do not present a communication interface. Nonetheless, this paper demonstrates that the coordination provided by the GCBC is not affected by the existence of Type A nd-DERs in the MG. At last, it is highlighted that the GCBC considers all DERs to be driven as current sources [46] (i.e., under a current-controlled mode) to achieve the facilitated compliance with the grid codes [47].

Table 1. Types of DERs considered for the MG and their control functionalities.

		Dispatchable	Communication (Remote Control)	Active Control	Reactive Control	Harmonic Control
nd-DER	Type A	X	X	✓	X	X
	Type B	X	✓	✓ [†]	✓	✓
d-DER	✓	✓	✓	✓	✓	

[†] Not performed under coordinated control.

The MG energy management is then explained based on the structure presented in Figure 2. A hierarchical management architecture based on multi-rate control [44] is considered for implementing the current-based coordination provided by the GCBC strategy. Three main control layers are responsible for the entire operation of the MG and

its interaction with the distribution system, being slightly different from classic hierarchical topologies found in the literature [12,48,49], as thoroughly explained in [43,44].



Figure 2. MG hierarchical control architecture with the integration of GCBC strategy.

The primary layer is where all the local controllers and operation algorithms are located to provide an adequate interconnection of DERs to the electric grid. Basic operational algorithms, such as the ones for grid synchronization and current/voltage control loops, as well as other specific embedded functionalities (e.g., MPPT control, anti-islanding, V-f droop control, etc.) are implemented within this layer at each DER. For the DERs coordinated by the GCBC strategy, control setpoints (α) are sent by the MGCC to regulate the output current at their point of connection (PoC), as explained in Section 2.1. Hence, the secondary control layer shown in Figure 2 incorporates the GCBC strategy and it is implemented within the MGCC. Such a layer is responsible for offering multiple MG functionalities, such as active, reactive, and harmonic current sharing among the DERs, control of the MG power dispatchability, and many other functionalities to achieve a more robust MG operation. Finally, the tertiary layer allows the MGCC to interact with the external market or regulatory players, allowing it to respond to external energy demands, as well as providing the intelligent and/or optimal management of the MG elements. For instance, based on the dispatchability setpoints (I^{Grid*}) established in agreement with the DSO, the tertiary layers allow the MG to regulate the power flow at its PCC, consequently supporting its participation in transactive actions [50].

2.1. The Generalized Current-Based Control Strategy

First we suppose that a number J (i.e., $j = 1, 2, 3, \dots, J$) of DERs exist in the grid-connected MG. Moreover, as long as the DERs present remote control capabilities, they can be controlled by the GCBC. Now, to explain the GCBC strategy, let us consider that the peak value (I) of current components from a DER and from the MG PCC will be denoted by I^{DER} and I^{Grid} , respectively. Additionally, one fundamental definition is highlighted: supposing a time-domain current ($i(t)$) composed of H harmonic components (i.e., $h = 1, 2, 3, \dots, H$), $i(t)$ can be rewritten at any time by Equation 1. Such a definition considers an AC time-domain signal of unity amplitude that determines the in-phase ($x_{h\parallel}$) or quadrature ($x_{h\perp}$) synchronism of the current components, respectively, in relation to the voltage of that same node of the circuit.

$$i(t) = \sum_{h=1}^H (I_{h\parallel} \cdot x_{h\parallel}(t) + I_{h\perp} \cdot x_{h\perp}(t)) \quad (1)$$

The GCBC strategy relies on three main tasks to coordinate DERs, being: (i) the local evaluation of electrical quantities at DERs and PCC; (ii) the processing of the GCBC algorithm at the MGCC; and (iii) the local current reference setting at DERs. The scheme shown in Figure 3 illustrates how these tasks compose the GCBC strategy. Note that, given a control cycle “ k ”, the GCBC tasks are processed sequentially at different locations of the MG, using communication links to adjust the currents injected by the DERs at the final step.

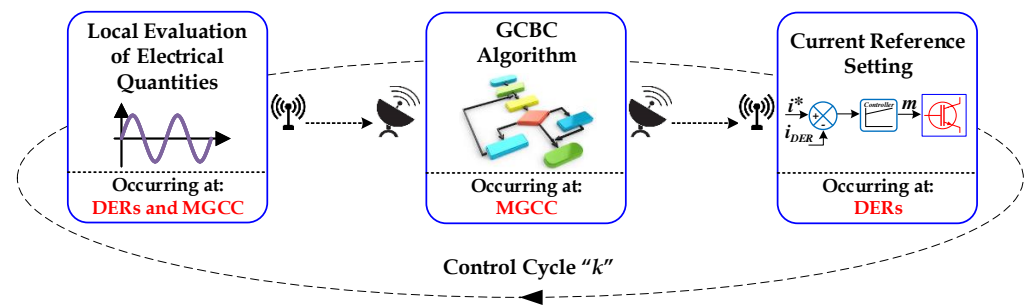


Figure 3. Three main tasks of the GCBC strategy.

Consequently, load changes and uncertainty in generation capabilities can be handled by the GCBC strategy, steering DERs to achieve the intended MG operational goals respecting their nominal capabilities. Let us now present a more detailed explanation about each of these tasks.

(i) *Local Evaluation of Electrical Quantities*

This task processes the electrical quantities (i.e., voltage and currents) at the nodes of interest. It occurs at each coordinated DER as well as at the MGCC. Such a procedure is required to detect the peak values of the currents flowing through the DERs' PoCs and the PCC. For instance, taking the time-domain local output current of a DER, $i_m^o(t)$, in which m stands for the respective phase of a generic circuit (e.g., $m = a, b$, or c , for three-phase topology). The scheme demonstrated in Figure 4a extracts the magnitude of the in-phase ($I_{h||m}^o$) and quadrature ($I_{h\perp m}^o$) currents components from $i_m^o(t)$. Because such calculations occur at the DERs and the PCC, one finds that $I_{h_m}^o = I_{h_m}^{DERj}$ for each j -th DER, and $I_{h_m}^o = I_{h_m}^{Grid}$ for the PCC.

The decomposition of current components should be conducted for all harmonic orders (h) aimed to be controlled. By managing the fundamental in-phase component, $I_{1||m}^o$, active current control is obtained, whereas reactive current control relates to $I_{1\perp m}^o$. The components of higher harmonic orders (i.e., for $h = 2, 3, 4, 5, \dots, H$), $I_{h||m}^o$, and $I_{h\perp m}^o$, are responsible for the regulation of non-fundamental currents. As a result, at this point, it is evident that a per-phase analysis of currents is performed by the GCBC at selected harmonic orders. It is important to reinforce that both even and odd harmonics can be considered in the GCBC formulation. Hence, the set of controlled harmonic orders is defined by the MGCC according to the MG's desired goals of operation.

The GCBC's local evaluation task first measures the local currents and voltages (v_m^o) of a PoC or PCC, as seen in Figure 4a (i.e., $v_m^o = v_m^{DERj}$ for DERs, or $v_m^o = v_m^{Grid}$ for the PCC). Later, the voltage feeds a PLL algorithm, allowing to obtain the fundamental synchronization angle θ_{1m} , which is also used for calculating the synchronization angles $\theta_{hm} = h \cdot \theta_{1m}$ that provide the references for the harmonic frames. By feeding such angles to cosine and sine functions, the unity reference signals, $x_{h||m}$ and $x_{h\perp m}$, can be obtained for the in-phase and quadrature orientations. Assuming that the adopted PLL algorithm is robust, the GCBC can endure operation under non-ideal voltage conditions. Hence, the PLL algorithm discussed in [51] is herein considered for the GCBC implementation.

Knowing $x_{h||m}$ and $x_{h\perp m}$, as well as the node current $i_m^o(t)$, a discrete Fourier transform (DFT) [52] allows to calculate the peak values of the targeted current components. The adopted DFT is devised in Figure 4a by means of moving average filters (MAFs) that act as low-pass filters (LPFs), allowing simple digital implementation. Consequently, due to the feature of this implementation, the peak current terms $I_{h||m}^o$ and $I_{h\perp m}^o$ are average quantities that could assume either positive or negative values, depending on how $x_{h||m}$ and $x_{h\perp m}$ interact with $i_m^o(t)$. For instance, attaining a positive value for $I_{1||m}^o$ would indicate an injection of active power. On the other hand, power absorption (i.e., storage) would result in a negative value for $I_{1||m}^o$. (The negative magnitude of a periodic current component

does not present mathematical meaning. Such a definition is an abstraction, given that the peak detection scheme from Figure 4 can indicate if a current component is either in phase or 180° shifted in relation to $x_{h||m}$ or $x_{h\perp m}$. For the case of having a 180°-shifted current signal, a negative peak value is obtained.) It is remarked that other approaches for the calculation of the peak currents [53,54] could be devised if desired, guaranteeing compatibility with the following steps of the GCBC strategy. Finally, note that in Figure 4b, a graphical representation of the discussed local evaluation is presented to further clarify how the peak currents are calculated.

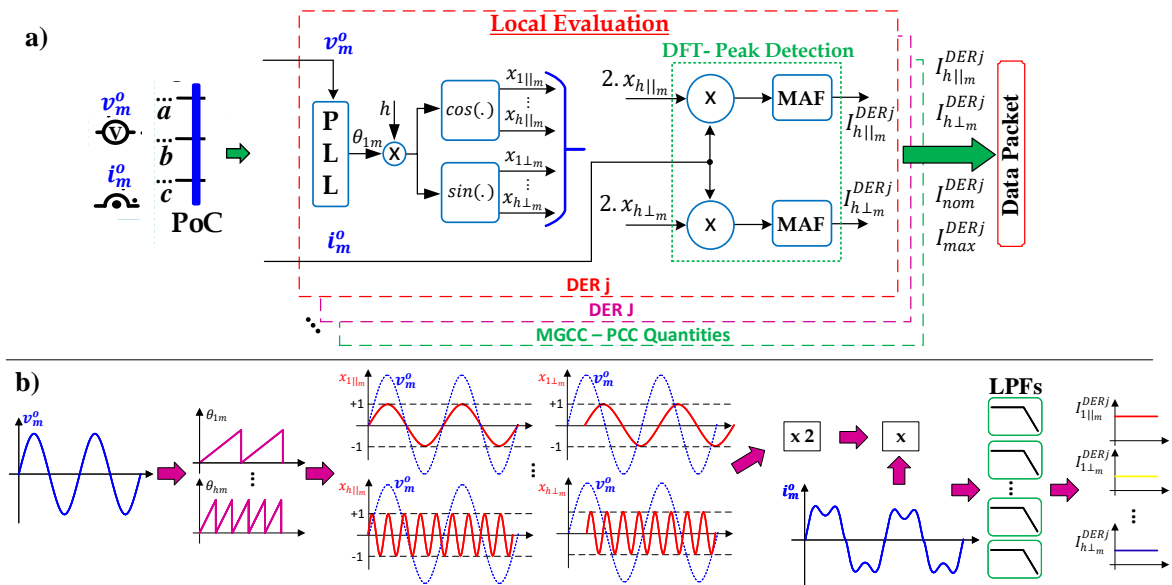


Figure 4. Task 1—Local evaluation of electrical quantities. (a) Decomposition scheme; and (b) illustration of the procedure in (a).

By having all the peak currents calculated (i.e., $I_{h||m}^o$ and $I_{h\perp m}^o$), they are gathered to compose a data packet, which is sent to the MGCC, as shown in Figure 4a. Along with the decomposed terms, other peak current terms are inserted into this data packet. Such quantities are the nominal current rating for each j -th DER ($I_{nom_m}^{DERj}$), the maximum active current that it can generate ($I_{1||max_m}^{DERj}$), and the maximum active current that it can store ($I_{1\perp max_m}^{DERj}$) if an ESS exists.

The term $I_{nom_m}^{DERj}$ relates to the nominal apparent power of that DER. Moreover, the term $I_{1||max_m}^{DERj}$ indicates j -th DER’s capability to inject active current, either considering the implementation of MPPT algorithms for its RES (i.e., if it is an nd-DER) or based on the usage of stored power (i.e., if it is a d-DER). On the other hand, the term $I_{1\perp max_m}^{DERj}$ relates to the SoC of the ESS, as typically adopted for battery systems [55], indicating that such a variable is only applied to d-DERs.

As a final remark, it is highlighted that $I_{h||m}^{Grid}$ and $I_{h\perp m}^{Grid}$ are only used locally by the MGCC. This occurs because they are obtained from quantities measured at the PCC and are not required to be transmitted to DERs at any moment.

(ii) *Processing of the GCBC Algorithm at the MGCC*

The second task relates to the operation of the GCBC algorithm at the MGCC. Such an algorithm needs to be periodically processed, taking into account the data packets transmitted by the DERs. In addition, the GCBC algorithm processing occurs at each control cycle “ k ” triggered at the beginning of a periodic window of the MG management, which operates between milliseconds and minutes, according to the control needs and physical topology of the system. Consequently, “ k ” is only updated at the next control

cycle “ $k = k + 1$ ”. By starting a new control cycle, after processing task “ i ”, the MGCC pulls the data packets processed by DERs and attains the results from the evaluation of the PCC currents.

By determining the H harmonic orders that need to be controlled, the following calculation is performed at the MGCC. The total current contribution of the J DERs is computed first, for each harmonic order h , being given by Equations (2) and (3). Note that the in-phase ($I_{h||m}^{DERt}$) and quadrature ($I_{h\perp m}^{DERt}$) current components are processed independently. In addition, the superscript “ t ” herein stands for the total quantities of the MG (i.e., with relation to all J DERs being coordinated).

$$I_{h||m}^{DERt}(k) = \sum_{j=1}^J I_{h||m}^{DERj}(k) \quad (2)$$

$$I_{h\perp m}^{DERt}(k) = \sum_{j=1}^J I_{h\perp m}^{DERj}(k) \quad (3)$$

Similarly, the nominal capabilities of the DERs ($I_{nom_m}^{DERj}$) need to be computed, along with their maximum generation ($I_{1||max_m}^{DERj}$) and storage ($I_{1||sto_m}^{DERj}$) currents, as given by Equations (4)–(6), respectively. The GCBC processing at this stage allows to identify the actual participation of DERs in the overall status of the MG operation.

$$I_{nom_m}^{DERt}(k) = \sum_{j=1}^J I_{nom_m}^{DERj}(k) \quad (4)$$

$$I_{1||max_m}^{DERt}(k) = \sum_{j=1}^J I_{1||max_m}^{DERj}(k) \quad (5)$$

$$I_{1||sto_m}^{DERt}(k) = \sum_{j=1}^J I_{1||sto_m}^{DERj}(k) \quad (6)$$

Because the MGCC also has the information about the currents flowing through the PCC (i.e., $I_{h||m}^{Grid}$ and $I_{h\perp m}^{Grid}$), the summed current contribution ($I_{h||m}^L$ and $I_{h\perp m}^L$) of all MG elements, including the passive or non-controlled ones, can be devised by Equations (7) and (8). For that, Kirchhoff’s current law can be applied at the MG PCC as presented in Figure 5.

$$I_{h||m}^L(k) = I_{h||m}^{DERt}(k) + I_{h||m}^{Grid}(k) \quad (7)$$

$$I_{h\perp m}^L(k) = I_{h\perp m}^{DERt}(k) + I_{h\perp m}^{Grid}(k) \quad (8)$$

Additional remarks are made with regard to $I_{h||m}^L$ and $I_{h\perp m}^L$. First, note that they not only comprise the currents drawn by the loads that may exist within the MG, but they also incorporate all the power losses occurring in line impedances and other dissipative elements. Moreover, DERs not being coordinated by the GCBC strategy are also considered within these terms. Yet, Equations (7) and (8) are only valid due to the limited size of the considered MG, its homogeneous characteristic, and the low X/R feature of its line impedances, which guarantees that voltage shifts are not significant [43]. As a last remark, note that if the DERs share $I_{h||m}^L$ and $I_{h\perp m}^L$ completely, the current flow through the PCC will become null. Therefore, if $I_{h||m}^L = 0$ and $I_{h\perp m}^L = 0$ for all significant harmonic orders, the MG operates under full self-consumption mode [56] in a steady state, not depending on the upstream grid (i.e., aside from the fact of forming the grid by imposing the voltages and frequency at the PCC).

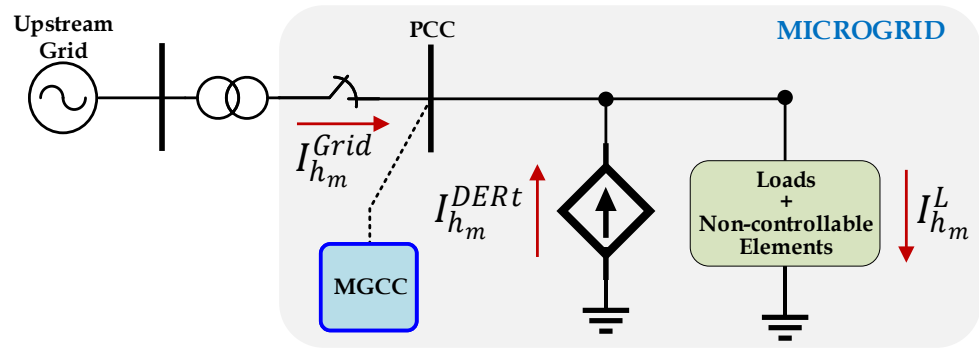


Figure 5. Kirchhoff’s current law applied to the MG peak current analysis.

Now, the controllable power dispatchability through the PCC provided by the GCBC is further explained. Such a desired power flow can be translated into current signals that must be drawn or dispatched by the MG, considering that it is interpreted as single entity from the upstream grid perspective. Such reference signals refer to each harmonic order “ h ” at the PCC, namely $I_{h||m}^{Grid*}$ and $I_{h\perp m}^{Grid*}$, and they establish the amount of peak current that must circulate at the PCC, even after fulfilling the MG internal current needs (i.e., $I_{h_m}^L$). Consequently, $I_{h||m}^{Grid*}$ and $I_{h\perp m}^{Grid*}$ are usually set by the DSO. For example, if $I_{1||m}^{Grid*}$ is a non-null positive quantity, the upstream grid interprets the MG behaving as a single entity acting as a load drawing active currents. On the other hand, if $I_{1||m}^{Grid*}$ is a negative quantity, it means energy export (i.e., the MG dispatching active power). In addition, as typically adopted in MG contracts, active and reactive power is limited [57]. Consequently, such PCC reference terms are constrained to upper and lower bounds (i.e., $\underline{I_{1_m}^{Grid}}$ and $\overline{I_{1_m}^{Grid}}$) and Equations (9) and (10) must be considered.

$$\underline{I_{1||m}^{Grid}} \leq I_{1||m}^{Grid*} \leq \overline{I_{1||m}^{Grid}} \quad \forall I_{1||m}^{Grid*} \in \mathbb{R} \tag{9}$$

$$\underline{I_{1\perp m}^{Grid}} \leq I_{1\perp m}^{Grid*} \leq \overline{I_{1\perp m}^{Grid}} \quad \forall I_{1\perp m}^{Grid*} \in \mathbb{R} \tag{10}$$

The GCBC algorithm then allows to define the currents that need to be shared by the DERs, at the next control cycle “ $k + 1$ ”, namely $I_{h||m}^*(k + 1)$ and $I_{h\perp m}^*(k + 1)$. Such references can be calculated according to Equations (11) and (12), which are expanded to Equations (13) and (14).

$$I_{h||m}^*(k + 1) = I_{h||m}^L(k) - I_{h||m}^{Grid*}(k + 1) \tag{11}$$

$$I_{h\perp m}^*(k + 1) = I_{h\perp m}^L(k) - I_{h\perp m}^{Grid*}(k + 1) \tag{12}$$

$$I_{h||m}^*(k + 1) = I_{h||m}^{DERt}(k) + I_{h||m}^{Grid}(k) - I_{h||m}^{Grid*}(k + 1) \tag{13}$$

$$I_{h\perp m}^*(k + 1) = I_{h\perp m}^{DERt}(k) + I_{h\perp m}^{Grid}(k) - I_{h\perp m}^{Grid*}(k + 1) \tag{14}$$

Hence, to coordinate DERs to achieve current sharing over multiple harmonic orders, $I_{h||m}^*$ and $I_{h\perp m}^*$ are used to calculate scaling coefficients (i.e., namely $\alpha_{h||m}$ and $\alpha_{h\perp m}$), by means of Equations (15) and (16). The term $\sqrt{\Delta I_m}$ is the overall peak current capability of the MG, and it provides proportional current sharing among DERs, while respecting their current ratings. This term must be adjusted iteratively according to the calculation of each scaling coefficient, as demonstrated in Figure 6.

$$\alpha_{h||m} = \frac{I_{h||m}^*(k + 1)}{\sqrt{\Delta I_m}}, \quad \forall \alpha_{h||m} \in \mathbb{R} : -1 \leq \alpha_{h||m} \leq +1 \tag{15}$$

$$\alpha_{h\perp m} = \frac{I_{h\perp m}^* (k+1)}{\sqrt{\Delta I_m}}, \quad \forall \alpha_{h\perp m} \in \mathbb{R} : -1 \leq \alpha_{h\perp m} \leq +1 \quad (16)$$

Such a correction of $\sqrt{\Delta I_m}$ follows a sequential order, having active current control processed first, reactive control next, and the in-phase and quadrature harmonic orders processed last. Particular attention must be given to active current control because active current injection or absorption must be related to $I_{1||\max m}^{DERt}$ and $I_{1||sto m}^{DERt}$, respectively. Note that, because each step of this procedure is based on orthogonal subtractions, by using the DERs' estimated currents (i.e., given by $\hat{I}_{h||m}^{DERt} = \alpha_{h||m} \cdot \sqrt{\Delta I_m}$ or $\hat{I}_{h\perp m}^{DERt} = \alpha_{h\perp m} \cdot \sqrt{\Delta I_m}$) at "k + 1", overcurrents are prevented. Additionally, such phasorial calculations also guarantee that their current capabilities are respected. The scheme in Figure 6 uses two auxiliary variables (ΔI_m and $\Delta I_{m,old}$), which hold the quadratic value of the overall current capability at the actual and previous calculation steps, respectively. It should ultimately be remarked that, if desired, for whatever MG management reason, the sequence of the iterative calculation of $\sqrt{\Delta I_m}$ can be flexibly readjusted.

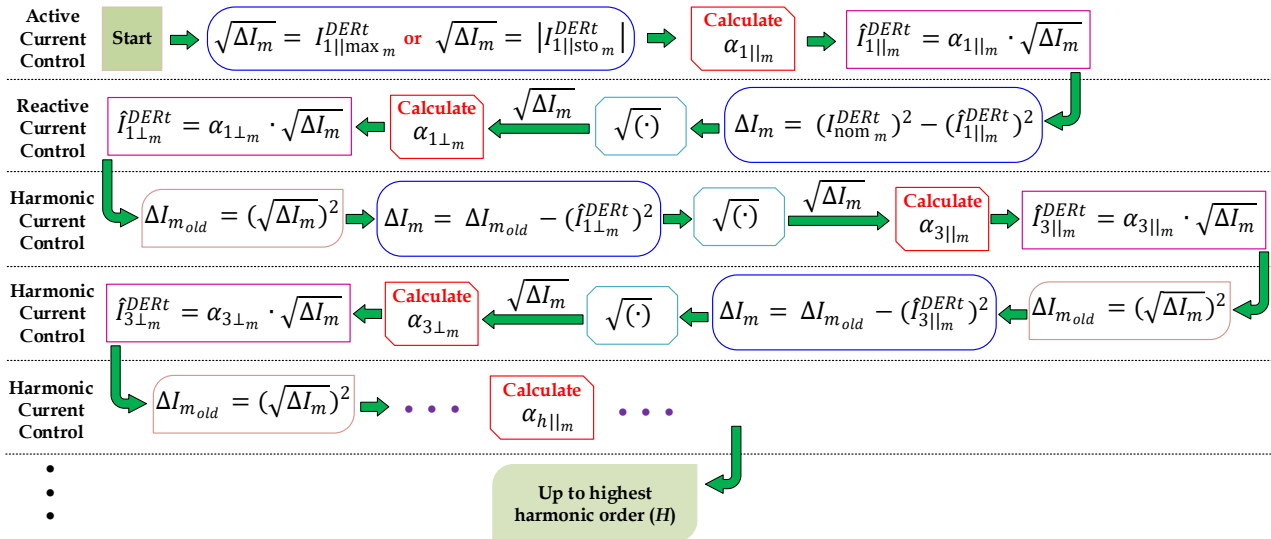


Figure 6. Iterative calculation of DERs' current capability ($\sqrt{\Delta I_m}$).

Finally, further explanations are given about the scaling coefficients, $\alpha_{h||m}$ and $\alpha_{h\perp m}$. These coefficients are within the range of $[-1, +1]$, and if they are equal to $+1$ or -1 , it indicates that all the DERs' current capacity, at a given harmonic order h , is used. As expected, if these coefficients are null, no current control is performed at the respective harmonic order. In particular, when looking into the coefficients of the fundamental order, one can generally understand the coordination purpose of the DERs.

For instance, the term $\alpha_{1||m}$ relates to active current control, and it indicates that power injection is demanded by the DERs (i.e., if $\alpha_{1||m} > 0$), or that absorption/storage is commanded (i.e., if $\alpha_{1||m} < 0$). On the other hand, the term $\alpha_{1\perp m}$ implies that inductive or capacitive behavior is provided by the DERs, if $\alpha_{1\perp m} > 0$ or $\alpha_{1\perp m} < 0$, respectively. Yet, by using the non-fundamental scaling coefficients (i.e., $\alpha_{h||m}$ and $\alpha_{h\perp m}$, for $h \geq 2$), the MG manager has a means to implement distributed and selective compensation of harmonic currents. Of course, for the case of nd-DERs not comprising ESS, $\alpha_{1||m}$ cannot assume negative values, as $I_{1||sto m}^{DERj}$ is null. In addition, because the GCBC algorithm can also be employed to coordinate active filters [58], a similar idea would apply, resulting in $\alpha_{1||m}$ being always null, as $I_{1||\max m}^{DERj} = I_{1||sto m}^{DERj} = 0$.

This task of the GCBC strategy terminates by gathering, in a data packet, the scaling coefficients of all harmonic orders to be controlled. Sequentially, this data packet is broad-

cast to all participating DERs within the MG, so they can adjust their output currents as given by the next step of the GCBC approach.

(iii) *Current Reference Setting at DERs*

The final procedure of the GCBC strategy is responsible for setting the right current references to be injected by the DERs. This task occurs only at each DER, and it uses the scaling coefficients transmitted by the MGCC. Let $i_m^{DERj*}(t)$ be the time-domain current reference of the phase m , for each j -th DER participating in the coordination strategy. Such a reference can then be constructed similarly to Equation (1), in which the unity reference signals (i.e., $x_{h||m}^{DERj}$ and $x_{h\perp m}^{DERj}$) come from the local evaluation of the electrical quantities realized by that j -th DER. Thus, the final current reference used for that DER is given by Equations (17) and (18), which can be summed up to result in Equation (19), similarly to Equation (1).

$$i_{||m}^{DERj*}(t) = \sum_{h=1,2,3,\dots}^H \left(\alpha_{h||m} \cdot \sqrt{\Delta I_m^{DERj}} \cdot x_{h||m}^{DERj}(t) \right) \quad (17)$$

$$i_{\perp m}^{DERj*}(t) = \sum_{h=1,2,3,\dots}^H \left(\alpha_{h\perp m} \cdot \sqrt{\Delta I_m^{DERj}} \cdot x_{h\perp m}^{DERj}(t) \right) \quad (18)$$

$$i_m^{DERj*}(t) = i_{||m}^{DERj*}(t) + i_{\perp m}^{DERj*}(t) \quad (19)$$

In such equations, the current capability of each respective DER ($\sqrt{\Delta I_m^{DERj}}$) is used. This variable is calculated in the same way as for the total current capability of the MG ($\sqrt{\Delta I_m}$), following the same iterative scheme presented in Figure 6. However, for $\sqrt{\Delta I_m^{DERj}}$, only the local quantities of that specific j -th DER must be used (i.e., $I_{nom_m}^{DERj}$, $I_{1||max_m}^{DERj}$, and $I_{1||stom_m}^{DERj}$).

A final remark is made with regard to the per-phase controllability provided by the GCBC strategy. Note, from Equation (19), that the current reference for a DER is locally constructed based on the evaluations performed at each phase m , even for the three-phase topology. This indicates that, for the case of single-phase MGs, the GCBC is performed only for one phase. On the other hand, for three-phase MGs, the GCBC application depends on the topology of the inverters. For instance, if three-leg DERs exist, only two phases need to be controlled [59], being the modulation of the third leg obtained from Kirchhoff's current law. Hence, the GCBC needs to be implemented considering two phases to adequately coordinate such DERs. For the case in which three-phase four-leg DERs exist (i.e., in a three-phase four-wire MG) [44], the GCBC is applied to three phases, controlling the DER's neutral leg by Kirchhoff's current law.

3. Microgrid Experimental Prototype

A single-phase laboratory-scale MG prototype is used as the main platform to perform the experimental validations within this paper. The equivalent circuit of the single-phase MG prototype is depicted in Figure 7. Moreover, a picture of the entire MG prototype is presented in Figure 8. A more detailed explanation about the implementation of each of the MG elements can be found in [60].

A 30 kVA AC grid emulator, model TC-ACS-30-528-4WR, forms the upstream grid, which is coupled to the MG PCC. Line impedances are used to interconnect the MG nodes (Z_{L1} to Z_{L5}), having $Z_{L1} = Z_{L2} = Z_{L3} = Z_{L4} = 2$. $Z_{L5} = 0.5$ mH. Three loads are considered for the MG operation, one being composed of an IT8616 electronic load (Z_{L1}) from ITECH[®] (i.e., emulating a constant 16 Ω resistor) and two passive loads, one an inductive load ($L_2 = 40$ mH) and the other a non-linear load (L_3). The MG prototype was emulated considering line-to-neutral grid voltage of 127 V_{RMS} at 60 Hz.

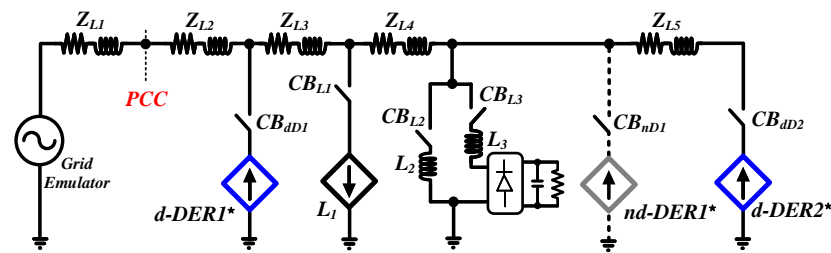


Figure 7. Equivalent circuit of the single-phase MG prototype assembled for experimental results.

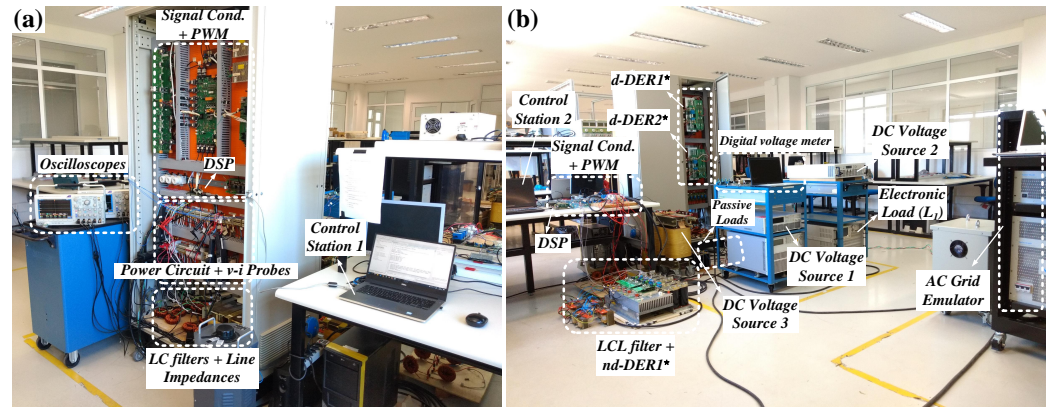


Figure 8. Experimental prototype of the single-phase MG: (a) front and (b) back views.

A full-wave diode rectifier having an inductor (5 mH) at its AC side constitutes the non-linear load, which has a capacitor bank (2.35 mF) in parallel with a resistor (41.8 Ω) at its DC side. Circuit breakers implemented in the MG allow all elements to be switched on or off (CB_{\cdot}). For the operational visualization, DPO3000 TEKTRONIX[®] oscilloscopes were used for acquiring current and voltage waveforms, and a DPO3PWR power analysis module was used to quantify the amplitude of harmonic components and the phase shift between voltage and current.

The MG presents three inverters, in which two of them are controlled as dispatchable units (i.e., d-DEI: d-DEI₁ and d-DEI₂), being ruled by the GCBC strategy. The third inverter operates as a Type A non-dispatchable unit (i.e., nd-DEI₁), only injecting active power into the MG when desired and not participating in the GCBC approach. When a Type B nd-DEI is needed in the experiments, d-DEI₁ emulates such a behavior instead of being a dispatchable element. The d-DEIs present LC output filters, while nd-DEI₁ uses an LCL output filter with passive damping resistor (R_d). The DEIs are driven as controlled current sources, and they use proportional-resonant (PRes) current controllers modeled as in [61]. Constant DC voltage sources are placed at the DC buses of the DEIs.

The two d-DEIs are controlled by a TMS320F28335 digital signal processor (DSP) from Texas Instruments[®], which processes the current controllers of both inverters and the code required for implementing the GCBC strategy. The nd-DEI₁ runs based on another independent TMS320F28335 DSP. The DEIs' parameters are presented in Table 2, being later described in [60]. The communication between the MGCC and DEIs required by the GCBC (i.e., transmission of data packets) was emulated to occur at each 16.66 ms (i.e., one cycle of the fundamental grid frequency).

Table 2. Parameters of DERs in the single-phase MG prototype used for experiments.

Parameter	Value
d-DERs	
d-DER ₁ nominal peak current	15 A _{pk} (≈3 kVA)
d-DER ₂ nominal peak current	20 A _{pk} (≈4 kVA)
Nominal current ratio between d-DERs ($r_{dDERs} = 20/15$)	1.33
LC filter: L_i and C_f	3.0 mH and 2.2 μF
Switching and sampling frequencies	12 kHz
DC link voltage (V_{DC})	270 V _{DC}
nd-DER	
nd-DER ₁ nominal peak current	15 A _{pk} (i.e., ≈3 kVA)
LCL filter—Inductors: L'_i and L_g	1.0 mH and 1.0 mH
LCL filter—Capacitor (C'_f) and Damping Resistor (R_d)	3.3 μF and 1 Ω
Switching and sampling frequencies	18 kHz
DC link voltage (V_{DC})	270 V _{DC}

To demonstrate MG operation when DERs are disabled and the loads are connected to the circuit, a preliminary result is shown in Figure 9. Such a result shows that, although the MG presented sinusoidal voltages at the PCC, the current demanded by the loads was distorted and phase shifted in relation to the voltages. The quantization seen in Table 3 forms a baseline for comparisons with the experiments in Section 4. In addition, it shows that the MG presents a considerable amount of active, reactive, and distortion powers circulating at the PCC, as well as a low power factor (i.e., mainly due to the circulation of reactive power). The harmonic components of the PCC currents seen in Table 3 indicate that, beyond the fundamental term, the most significant harmonic orders causing current distortion are the odd ones, from the 3rd up to the 9th. The total harmonic distortion (THD_i) of the PCC current, caused by the loads, was 19.5%. Yet, the power measurements adopted herein in this paper are calculated according to the Conservative Power Theory (CPT) [62].

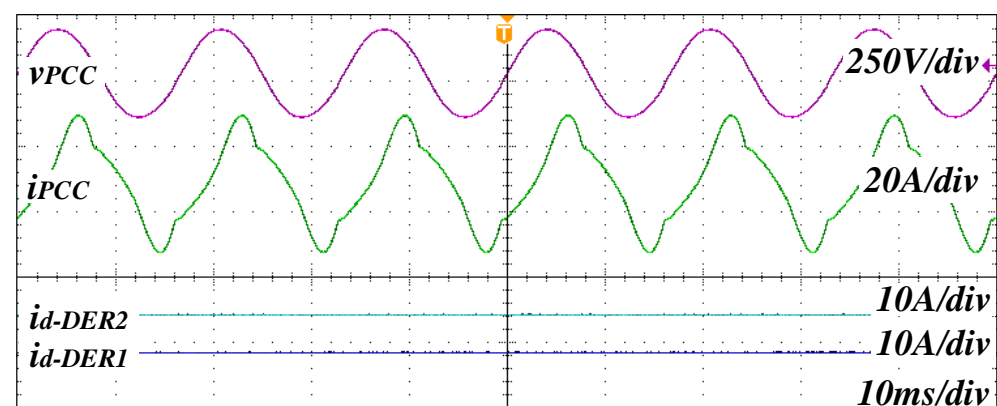
**Figure 9.** Experimental result: single-phase MG operating with all loads connected and with DERs disabled. From top to bottom: PCC voltage and current, d-DER₂ and d-DER₁ currents.

Table 3. Power and harmonic current measurements at the PCC for Figure 9.

PCC Powers	
Apparent (A)	1501 VA
Active (P)	980 W
Reactive (Q)	1148 VAR
Distortion (D)	315 VA
PF	0.65
Harmonic Amplitude	
$h = 1$	12.2 A _{RMS}
$h = 3$	2.31 A _{RMS}
$h = 5$	0.63 A _{RMS}
$h = 7$	0.26 A _{RMS}
$h = 9$	0.19 A _{RMS}

4. Experimental Results of the DER Coordination under Adverse Scenarios

Having presented the introductory discussions about the MG operation, and based on the explanations previously provided about the operational features of the GCBC strategy, this section addresses the experimental validations intended within this paper by means of four study cases.

First, it is demonstrated in Study Case I (in Section 4.1) how DERs of a different operational nature are coordinated by the GCBC, also considering challenging dynamic conditions, such as when variable generation capabilities occur. The adverse scenario having DERs of limited power ratings is later presented in Study Case II (in Section 4.2), demonstrating how the dynamic saturation provided by the GCBC allows to respect the DERs' power capabilities. Finally, in Sections 4.3 and 4.4, the voltage quality complications related to the existence of distortions and the need for voltage ride-through capabilities are addressed, respectively, by Study Cases III and IV.

4.1. Study Case I: DERs of Different Operational Natures and Variable Generation Capabilities

By employing the GCBC strategy for energy management, it is important to understand how the existence of DERs of a varied nature (i.e., being nd- and d-DERs) possibly affects the MG operation. In addition, it is necessary to assess how the control strategy performs when DERs face variable energy generation profiles. Hence, the experimental validations are herein presented based on the MG prototype presented in Section 3. All linear and non-linear loads are connected to the MG at all moments (see Figure 7), and three different scenarios are considered for the operation of the DERs during this study case. It is highlighted that, when non-fundamental current sharing is targeted, the 3rd and 5th harmonic orders are selected to be controlled by the GCBC in all the following experiments.

The first scenario is presented in Figure 10a. This case considers that d-DER₁ and d-DER₂ are the only DERs connected to the MG (i.e., nd-DER₁ is disconnected). With regard to their nature of operation, d-DER₁ is configured to be driven as a Type B nd-DER (i.e., only for this section). Its main goal is to inject its generated active current into the MG, having its remaining current capability allocated to other functionalities by means of the GCBC strategy. Consequently, d-DER₁ is coordinated along with d-DER₂ to share reactive and harmonic currents, if it has remaining capability. d-DER₂ has its active, reactive, and harmonic currents coordinated by the GCBC because it fully operates as a dispatchable inverter.

During the steady-state operation seen in Figure 10a, d-DER₁ is injecting the active current at 20% of its nominal rating. Note in Table 4, for instance, that d-DER₁ processes 251.3 W of active power (P). Consequently, the GCBC has to automatically adjust the steering of d-DER₂ to process the remaining active current measured at the PCC, making P reach a practically negligible value (i.e., -48.49 W—see Table 4) when compared to the

baseline of 980 W (see Table 3). Such a condition occurs because the GCBC is set to provide a null flow of active, reactive, and harmonic currents at the MG PCC.

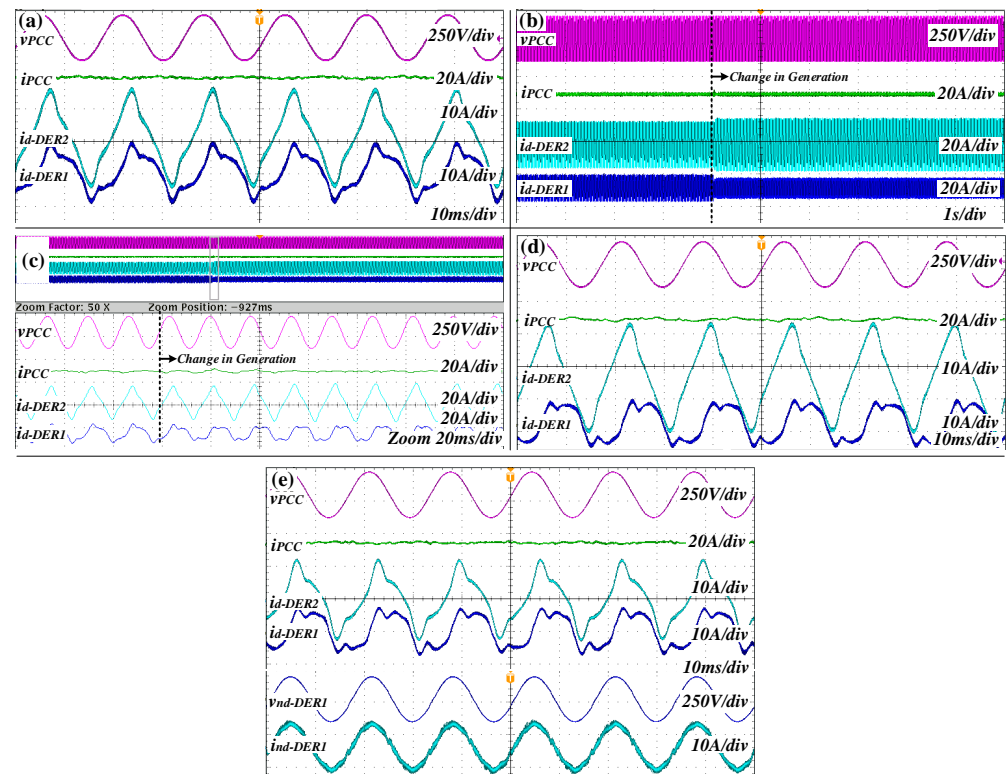


Figure 10. Experimental results: full current control with assorted inverters and variable generation capability. (a) d-DER₁ emulates an nd-DER with 20% of generation capability; (b) d-DER₁ emulates an nd-DER transiting from 20% to null generation capability; (c) zoom-in view of (b); (d) steady-state condition of (c); (e) case (d) considering nd-DER₁ injecting active power. From top to bottom: PCC voltage and current, d-DER₂ and d-DER₁ currents. The results in (e) were measured using two oscilloscopes using AC line trigger mode.

Table 4. Steady-state powers at the PCC and at DERs for Figure 10. Units: P (W), Q (VAR), and D (VA).

	Figure 10a			Figure 10d			Figure 10e		
	P	Q	D	P	Q	D	P	Q	D
PCC	−48.49	7.67	101.4	−36.0	47.1	77.9	−31.2	−16.9	110.4
d-DER ₂	826.5	647.8	203.3	1154	573.2	187.8	460.0	679.2	231.2
d-DER ₁	271.3	542.3	184.5	−7.5	584.5	176.3	9.51	556.5	169.6
nd-DER ₁	0.0	0.0	0.0	0.0	0.0	0.0	591.4	2.7	74.4

Because d-DER₁ has most of its power capability not being exploited, similarly to d-DER₂, the GCBC interprets that both DERs can cooperate to strive for the sharing of reactive and harmonic currents circulating within the MG. Hence, Figure 10a demonstrates that both of these DERs also inject currents that are phase shifted in relation to the PCC voltage, also being highly distorted, indicating the processing of reactive and harmonic components, respectively. Therefore, the current flow through the PCC becomes practically null, as expected for MGs operating under a self-consumption mode [56].

From this first scenario, it is important to highlight that the currents of both DERs are not proportional, as the inverters are playing different roles. The quantization shown in Table 4 also makes this condition evident, because both DERs process non-proportional values of P . Moreover, the processed reactive and harmonic powers do not appear to be

proportional at first sight. Nevertheless, the current-sharing proportionality provided by the GCBC should only be considered based on the remaining current capabilities of the DERs after the active power is processed. By analyzing the power terms from Table 4, a proportion ratio (r_{dDERs}) of 1.19 can be found for these two DERs. Thus, this result indicates that an adequate current sharing is provided by the GCBC, as a reference ratio of 1.21 can be theoretically calculated for the reactive and harmonic sharing during this scenario.

The second experimental scenario from this study case is presented in Figure 10b–d. Such results show the transient and steady-state operation of the MG, considering that the active current generation from d- DER_1 is reduced from 20% to 0%. Consequently, d- DER_1 starts to operate similarly to an active power filter (i.e., only processing non-active currents). The instant of such a change at d- DER_1 is depicted in 10b, and the zoom-in view of this transition is seen in Figure 10c. Note that such conditions do not cause disturbances in the PCC voltage nor in any of the currents under analysis. Moreover, it is evident that the GCBC takes approximately three cycles to adjust the DERs' currents to obtain the desired null current flow at the MG PCC.

The waveforms during the steady-state condition for this case are presented in Figure 10d. It shows that d- DER_1 's current is significantly different from d- DER_2 's, because the former only processes reactive and harmonic currents. However, the powers shown in Table 4 show that the GCBC allows proportional power sharing to be achieved for the reactive and harmonic components. For instance, one can calculate 1.38 kVA of the remaining capability for d- DER_2 (i.e., $\sqrt{1800^2 - 1154^2}$), which is close to the nominal capability of d- DER_1 (i.e., 1.34 kVA, see Table 2). As a consequence, the two inverters should process similar amounts of Q and D powers, which is indicated by the results in Table 2 (see that the DERs' non-active powers are practically the same).

The third scenario in this study case, the case in Figure 10e, is shown being complementary to Figure 10d. It demonstrates the interconnection of one nd- DER (i.e., nd- DER_1 —see Figure 7) to the MG while maintaining the same operating mode for d- DER_1 and d- DER_2 . Thus, nd- DER_1 operates injecting only active power (i.e., 591.4 W). Such a behavior can be noticed by nd- DER_1 's low distorted and in-phase current in Figure 10e, as well as by the power measurements in Table 2. Note that one more DER is providing the active currents drawn by the loads, the GCBC indirectly interprets such conditions at the PCC currents, being able to adjust the coordination of the coordinated DERs. Consequently, note that the currents from d- DER_1 and d- DER_2 present lower amplitudes than in Figure 10d, and the current flow through the PCC remains significantly low, as expected.

As a final comment, note that because d- DER_2 reduces its active power injection, its remaining current capability increases. Hence, the GCBC automatically leads d- DER_2 to process more reactive and harmonic currents than d- DER_1 (see the Q and D powers in Table 2). Nonetheless, such current sharing still occurs proportionally to the remaining capabilities of the two DERs, achieving $r_{dDERs} = 1.22$ (i.e., which is close to the 1.29 ratio expected for this case). Such results corroborate the targeted study goals of this paper because they prove that the GCBC strategy is capable of coordinating DERs of different operational natures existing in a dispatchable MG, also coping with additional adverse conditions, such as having DERs with different power generation profiles.

4.2. Study Case II: DERs with Limited Power Ratings

Microgrids are dynamic systems that constantly change their operational conditions due to the connection and disconnection of loads and DERs, requiring coordination strategies to rapidly adjust control setpoints in order to maintain the expected energy management goal. Moreover, adverse conditions such as the power generation intermittency may also cause the power demand to be higher than the MG's internal energy supply, which may lead to the overstress of DERs if saturation techniques are not implemented in their coordination. This study case, which has its experimental results shown in Figure 11, demonstrates that the features of the GCBC strategy discussed in Section 2.1 allow to saturate the participation of DERs to respect their available current capabilities at all times.

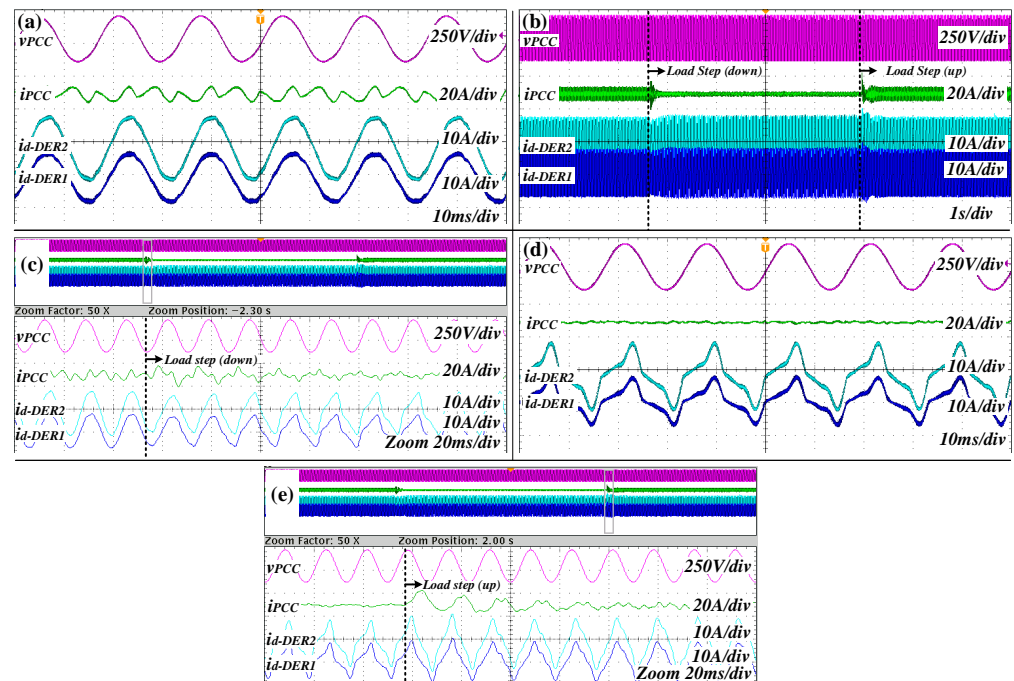


Figure 11. Experimental results: full current control under limited power capability. (a) d-DER₁ and d-DER₂ with 50% smaller ratings than nominal values in Table 2; (b) load steps applied disconnecting and connecting load L_2 ; (c) zoom-in view of stage one in (b); (d) steady-state condition of (c); (e) zoom-in view of stage two in (b). From top to bottom: PCC voltage and current, d-DER₂ and d-DER₁ currents.

The experiments from this study case consider that all loads, as well as d-DER₁ and d-DER₂ are connected to the MG prototype. Both d-DERs operate as dispatchable units during this case, and the nd-DER is not connected to the MG. To more easily demonstrate the saturation features of the GCBC, the nominal current ratings of the d-DERs are reduced by 50% (i.e., by changing the software configuration on the DSP). Consequently, d-DER₁ and d-DER₂ are considered to have 7.5 A_{pk} and 10 A_{pk} of the nominal current capabilities, respectively. In addition, similarly to Study Case I, the two d-DERs are coordinated by the GCBC intending to achieve the full share of the active, reactive, and selected harmonic currents drawn by the loads.

The steady-state behavior of the d-DERs' operation is then presented in Figure 11a. Such a result shows that the inverters face a condition in which there is insufficient current capability to completely share load currents (i.e., I_{nom}^{DERt} is limited) (see the load's demand in Table 3). For that reason, the current drawn from the upstream grid does not become null, as can be noted by the distorted currents circulating at the PCC in Figure 11a. This condition occurs because the GCBC algorithm saturates the currents processed by the d-DERs in order to respect their available capabilities. For instance, note that the inverters only process fundamental currents (see that the d-DERs' currents are sinusoidal and slightly phase shifted in Figure 11a). Such d-DER currents are composed by: (i) the loads' active current and (ii) around 84% of the loads' reactive current, which is not 100% due to the GCBC's saturation scheme.

Another proof of the adequate saturation provided by the GCBC is observed in Table 5. The powers calculated for this scenario show that mainly Q and D are measured at the PCC, indicating that the current being dispatched through the PCC cannot be fully shared by the d-DERs due to their limited capabilities. By comparing the results from Figure 11a with two baselines, as seen in Table 5, it becomes clear that Q is only partially shared by the inverters. In addition, no amount of the D is processed, indicating that the GCBC only assigned active and reactive current sharing to the d-DERs as a consequence of the

saturation scheme discussed in Figure 6. The two mentioned baselines refer to the load condition (shown in Table 3) and another scenario having the d-DERs sharing currents considering their original power ratings (shown in Table 2), respectively.

Table 5. Steady-state power terms at the PCC for Figure 11.

	PCC Powers				
	Loads	Baselines		This Section	
		Full Share	Figure 11a	Figure 11d	
A [VA]	1051	98.27	362.40	79.88	
P [W]	980	−73.30	−70.72	6.25	
Q [VAR]	1148	−14.05	184.6	−20.60	
D [VA]	315	65.70	304.6	73.66	

The GCBC's saturation scheme iteratively calculates the DERs' current capabilities before defining the scaling coefficients. Hence, if the inverters hypothetically had nominal ratings (I_{nom}^{DERt}) even lower than the ones considered during this study case, the strategy would saturate the current processing while assigning the active current sharing to the inverters. For the case of Figure 11a, d-DER₂ and d-DER₁ process 6.79 A_{RMS} and 5.18 A_{RMS}, respectively. Thus, proportional current sharing occurs, although they operate under limited capability (i.e., $r_{dDERs} = 1.31$), knowing that the baseline ratio was 1.33.

Let us now demonstrate how the saturation scheme tied to the coordination of the DERs operates during load transitions, taking as reference the results shown in Figure 11b–d. Such experiments demonstrate that the adverse condition of having inverters with limited power ratings does not affect the current sharing if the load demand is lower than I_{nom}^{DERt} . This is demonstrated by applying a load step to the MG, abruptly switching off the circuit breaker of the inductive load L_2 (see Figure 7), which reduces the amount of reactive current drawn within the MG. Note that, in Figure 11b and in the zoom-in view of this action in Figure 11c, the GCBC approach is able to adequately readjust the currents processed by the inverters.

Figure 11c shows that, even though the mechanical switching of the circuit breaker is slow, after a few fundamental cycles (i.e., approximately seven), the d-DERs share the load currents without causing overvoltages or overcurrents. Moreover, the inverters' capabilities, as well as their proportionality in current sharing, are also respected during transients. The steady-state condition of this new load scenario is shown in Figure 11d, in which it is visually seen that the PCC current is practically null. The power terms presented in Table 5 show that low amounts of P , Q , and D are measured at the PCC. Yet, proportional sharing is proved by the proportion ratio of 1.36 obtained during Figure 11d.

A final experiment is then conducted by switching on the load L_2 . The results for this case are shown in Figure 11b and in the zoom-in view of Figure 11e. Note that the inverters are able to ride through the disturbance caused by the mechanical switching of the referred circuit breaker, without losing effectiveness in proportional current sharing nor leading to overcurrents in the DERs. Taking approximately seven cycles after the circuit breaker is switched on, the MG returns to the steady-state condition of Figure 11a, respecting the capabilities of the inverters during the transition.

All in all, it has been demonstrated by such experiments that the GCBC saturation scheme of Figure 6 is efficient, because it allows to respect the DERs' current capabilities at all operating times. Despite the GCBC's satisfactory performance in such matters, the importance of implementing current/power saturators in the inner loops of the DERs to ensure proper local control and redundancy for the coordinated perspective is reinforced.

4.3. Study Case III: Distorted Voltages

Voltage harmonics are an important matter in LV electrical grids because they may lead weak power grids (e.g., such as LV MGs) to instability and may also cause low energy

efficiency [63]. In addition, for the scenario of interconnected LV MGs, it is known that voltage distortions may be propagated throughout the distribution grid [64]. Consequently, the coordination of DERs under such adverse conditions must be always evaluated prior to a real implementation.

This study case focuses on assessing the capability of the GCBC strategy with regard to the coordination of DERs when the upstream grid imposes distorted voltages at the MG PCC. For the following experimental results, the MG prototype from Section 3 is used, having all loads connected, as well as the two d-DERs operating at nominal ratings. In addition, the grid emulator is set to operate considering the nominal voltage of the MG while also adding 12.50% of the 3rd harmonic order to the voltage waveform (i.e., the instantaneous non-sinusoidal voltage was $v^{Grid}(t) = 127 \cdot \sqrt{2} \cdot \cos(\omega_o \cdot t) + 15.87 \cdot \sqrt{2} \cdot \cos(3 \cdot \omega_o \cdot t)$). Thus, such a configuration constituted the referred scenario of having background harmonics in the grid voltage.

The MG operates under distorted voltages and the GCBC strives for providing the full share of the active, reactive, and selected harmonic currents (i.e., from the 3rd and 5th orders), as depicted in Figure 12. Note in Figure 12a, for instance, that when the d-DERs are disabled, the grid voltage is significantly non-sinusoidal, resulting in the PCC current being slightly different from the one seen in Figure 9.

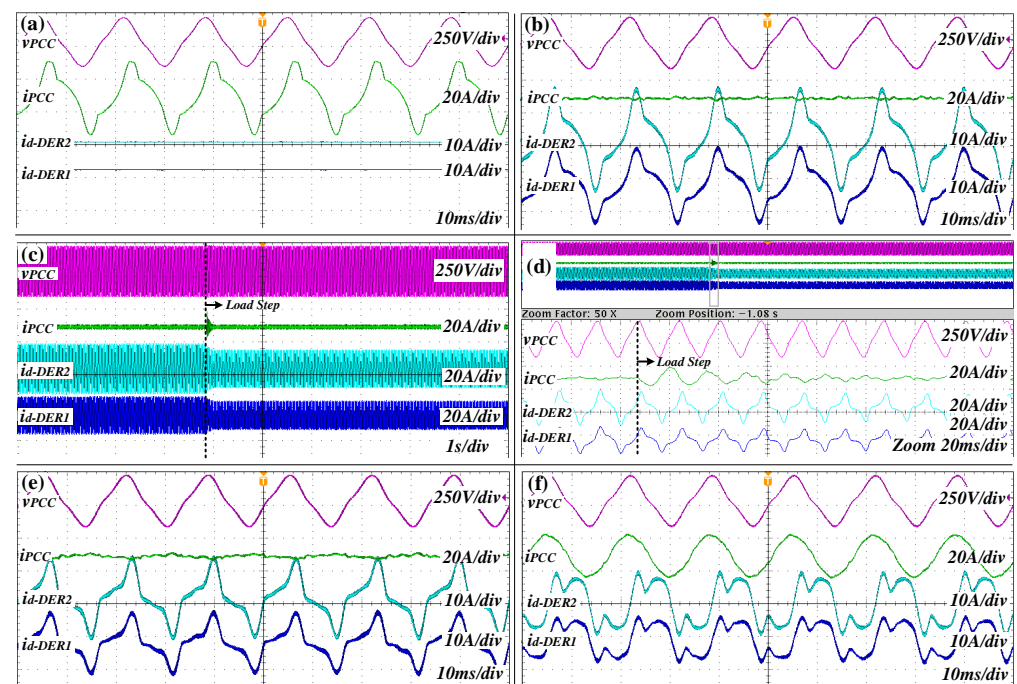


Figure 12. Operation of the GCBC strategy coordinating DERs under distorted voltages. (a) Grid voltage and current with DERs disabled; (b) active, reactive, and harmonic current-sharing functionality; (c) load step applied to (b) by disconnecting load L_2 ; (d) zoom-in view of (c); (e) steady-state condition of (d); (f) reactive and harmonic current-sharing functionality. From top to bottom: PCC voltage and current, d-DER₂ and d-DER₁ currents.

Now, Figure 12b shows the steady-state result for the MG operation considering that the GCBC is enabled and allowed the d-DERs to share the load currents. It is clear that a practically null PCC current results from the coordination of the inverters. The measurements presented in Table 6 also prove that the power flow through the PCC is practically negligible when compared to the load scenario of Figure 12a. Most importantly, although the grid voltage is distorted, a proportional sharing of currents occurs for the d-DERs, having d-DER₁ and d-DER₂ processing 6.00 A_{RMS} and 8.03 A_{RMS}, respectively, which reaches the expected ratio of 1.33. Thus, such a result proves that the GCBC resiliently

operates under such an adverse grid condition, without impacting the provision of the proportional current sharing to the inverters.

The transient response of the MG operating with distorted voltages is presented in Figure 12c–d, considering a load step in which the inductive load L_2 is switched off. Note in the results that, as soon as the load is disconnected, the GCBC starts adjusting the control coefficients. Consequently, the d-DETs' currents converge to steady state and remain in a stable condition. Figure 12d shows that the non-ideal voltage condition does not affect the adequate coordination of the inverters provided by the GCBC. For instance, observe that the steady-state operation is reached after approximately four cycles. The nominal capabilities of the d-DETs are respected and no current spikes occur at the inverters or at the PCC.

The steady state of this new operational condition is shown in Figure 12e. Note that a practically null current is drawn from the upstream grid, which leads to low amounts of the P , Q , and D powers measured at the PCC (see Table 6). In addition, the amplitude measurement of the currents at the PCC also shows that the cases from Figure 12b,e result in a similar current-sharing performance. Yet, because $r_{dDETs} = 1.30$ is obtained, it is proved that the expected proportional current sharing occurs.

A last experiment is shown in Figure 12f, demonstrating the coordination of the d-DETs while targeting only the distributed compensation of the reactive and the selected harmonic currents. This result shows that the GCBC is capable of steering inverters under non-sinusoidal voltages, offering the selective compensation of the current terms, allowing a low-distortion current that is practically in phase with the PCC fundamental voltage. The PCC current presented 1.03° of the phase shift, and it indicates that mainly active power is measured at the PCC. One can observe in Table 6 that the Q and D powers are significantly reduced for the case of Figure 12f, and P is practically not affected when compared to Figure 12a.

Table 6. Steady-state powers and current amplitudes at the PCC for Figure 12.

PCC Powers				
	Load (Figure 12a)	Full Control (Figure 12b)	Full Control (Figure 12e)	React. + Harm. Control (Figure 12f)
A [VA]	1543	83	121	1102
P [W]	957	−15	−82	1086
Q [VAR]	1157	−10	−23	−27
D [VA]	355	81	84	122
Harmonic Amplitude (A_{RMS})				
$h = 1$	12.3	0.13	0.74	8.94
$h = 3$	3.23	0.26	0.27	0.26
$h = 5$	0.99	0.14	0.19	0.18

As a final comment, this study case demonstrates a direct consequence of the GCBC formulation presented in Section 2.1, which relates to the terms $I_{h||}^*$ and $I_{h\perp}^*$ being obtained from the total portion of the load currents. Such terms lead to the selective compensation of harmonic currents, not taking into account voltage distortions. Therefore, this makes the GCBC offer the distributed compensation of harmonic currents resulting in sinusoidal currents at the PCC, regardless of the voltage distortions. Note that an MG is then seen by the upstream grid as a single controllable entity (e.g., load) that only draws sinusoidal currents. Such a behavior characterizes the sinusoidal current synthesis (SCS) concept [65,66], which has the advantage of providing low THD currents at the PCC. Nevertheless, it is also known that SCS-based strategies present limited capability to damp harmonic resonances, which may be an important concern to be accounted for, depending on the MG perspective.

4.4. Study Case IV: Voltage Ride-through Capability

The interconnection of DERs is becoming stricter day by day due to the inherent complications related to the coupling of switching power interfaces with LV electric grids [22]. Consequently, grid codes and standards have been updated in the past years [47,67,68], requiring DERs to offer more sophisticated operational functions, such as the capability to withstand voltage disturbances. In particular, with regard to the functionality of tolerating non-steady voltage profiles [47], namely ride-through capability, the DERs must not disconnect and maintain a resilient operation. Consequently, it is also expected from the single-controllable MG to stay connected to the main grid even under such voltage disturbances.

Thus, voltage sags, which cause lower voltage magnitudes (namely low-voltage ride through (LVRT)), and swells, which lead to higher voltage magnitudes (i.e., high-voltage ride through (HVRT)), should not negatively affect the MG controllability while emulating a single entity. In addition, such adverse conditions should also not affect the coordination of DERs, ensuring that they safely continue to pursue the expected MG goals. Hence, the GCBC strategy is assessed in this study case with regard to LVRT and HVRT capabilities.

Let us again consider the MG prototype from Figure 7 having the two d-DERs connected, as well as considering all the linear and non-linear loads. The experimental results are shown in Figure 13, knowing that the inverters are coordinated by the GCBC to share the active, reactive, and selected harmonic currents, at all instants. Moreover, because loads can be considered as constant impedances, their demanded currents vary proportionally to the voltage applied to them. The experiments in Figure 13 comprised two scenarios: (i) for the first one, the grid emulator imposes an abrupt voltage sag in the MG, forcing the GCBC to endure an LVRT condition, and (ii) for the second, a sudden voltage swell is applied to the MG, requiring the system to face the HVRT.

A general view of the MG operation transiting through the different voltage conditions is first provided in Figure 13a, in which three intervals can be observed on the profile of the PCC voltage (see purple waveform). During the initial interval, the nominal condition of the MG (i.e., grid voltage of 127 V_{RMS}) is seen, considering that the d-DERs are sharing currents and providing practically null current flow at the PCC. For the second interval, a sag of 13.33% is applied to the grid voltage, reaching 110 V_{RMS} (see the reduction in the amplitude for the purple waveform in Figure 13a). Observe that the control strategy allows the MG and DERs to ride through the change in voltage, returning to a stable steady-state operation. For the third interval, a swell is emulated in the MG voltage, its magnitude rising from 110 V_{RMS} to 141.10 V_{RMS}. It is evident in Figure 13a that, even though such a change in the voltage magnitude is of approximately 28%, the d-DERs keep sharing currents and reach a steady state without resulting in MG instability.

By calculating r_{dDERs} after the LVRT and HVRT transitions occur (i.e., after the steady state is reached), the values of 1.29 and 1.31 are obtained, respectively. Thus, because such results are very close to each other and are around the expected value, they show that the d-DERs' current sharing is still adequate, also demonstrating that voltage disturbances do not affect the overall performance of the MG operation, which remains operating stably. In addition, because the steady-state apparent power obtained at the PCC is 118.10 VA and 157.12 VA after the LVRT and HVRT events, respectively, it is also proved that the performance of the MG dispatchability is practically the same. It is important to highlight that, as expected, the obtained apparent power at the PCC is slightly higher for the HVRT because a voltage magnitude higher than the nominal value leads to higher current amplitudes.

In Figure 13b, more details are presented for the LVRT transition. This result shows that, as the voltage step is emulated, the d-DERs suffer an increase in the peak value of their instantaneous currents. This is indeed expected as the current controllers implemented during the experiments tend to maintain the power balance between the DC and AC sides of the inverters. Even though such an increase in currents during the LVRT can be avoided by implementing saturation algorithms [69] on the local controllers of the inverters, the results indicate a non-critical MG condition during this scenario. The maximum current values reached by d-DER₁ and d-DER₂ are 15.46 A and 16.76 A, respectively, which still

respect the nominal ratings of the inverters. Moreover, from Figure 13b, one can notice that, after two cycles, the current amplitudes are already similar to the previous scenario. Hence, the GCBC withstands the coordination of the d-DERs, reaching a steady state in approximately five cycles. Consequently, no significant impact is observed on the MG operation, apart from the transitions in the currents caused by the local controller of the d-DERs.

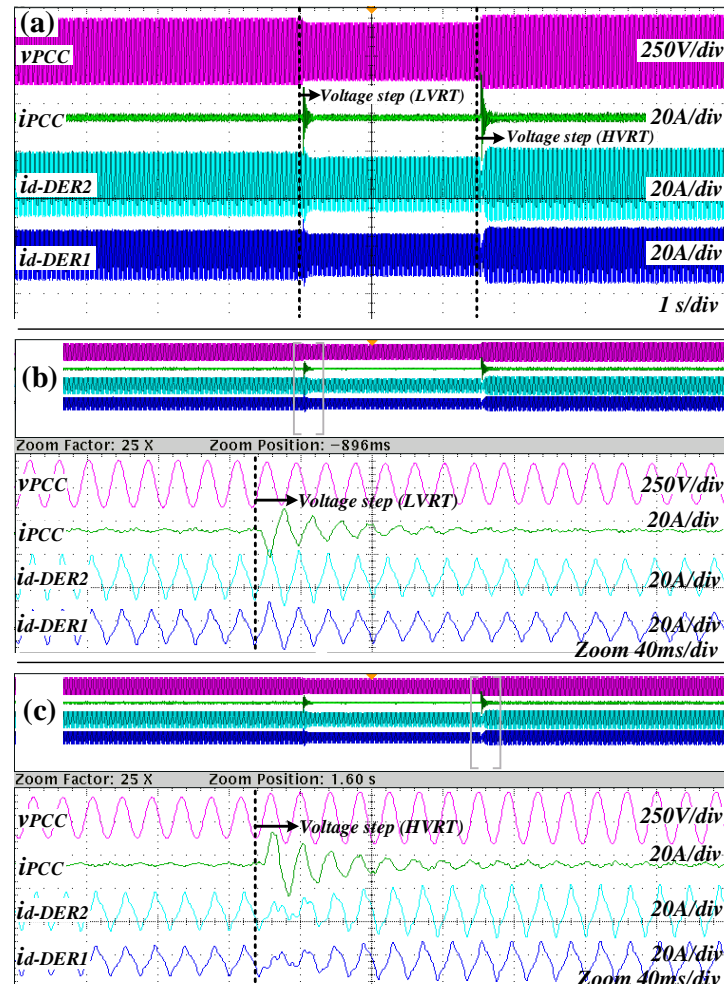


Figure 13. Experiments of the GCBC coordination considering voltage ride-through capabilities. (a) Steady-state view of voltage steps; (b) zoom-in view of a negative step in grid voltage; and (c) zoom-in view of a positive step in grid voltage. From top to bottom: PCC voltage and current, d-DER₂ and d-DER₁ currents.

At last, for the HVRT scenario seen in Figure 13c, the same resiliency is evidenced for the GCBC strategy. For instance, after the step increase in the grid voltage, the d-DERs take approximately five cycles to return to the steady-state operation, and the proportional current sharing is not ceased during the transition instants. Nevertheless, differently from the LVRT scenario, the transient behavior of the d-DERs' local controllers leads to a reduction in the current injection, as the magnitude of their PoC voltages increase. The GCBC strategy is again able to adequately ride through the voltage swell. If saturation algorithms were incorporated into the local controllers of the DERs, no impact would occur on the overall coordinated operation, as the GCBC algorithm only processes and controls the average values of the currents measured within the MG. The results of this study case then prove that the GCBC strategy allows to adequately coordinate DERs and maintain the MG operating as a single-controllable entity, even if the voltages may suffer adverse conditions, such as sags and swells.

5. Conclusions

This paper presents discussions and experimental validations to demonstrate that the GCBC strategy previously proposed in [43–45] is capable of adequately coordinating DERs in a grid-connected LV MG under adverse conditions. It is demonstrated that such a control strategy allows to steer DERs of dispatchable and non-dispatchable natures, being flexible to handle the intermittency from RES-based generation systems and also supporting a stable MG operation when DERs without communication interfaces are present. In addition, laboratory experiments show that the GCBC's saturation strategy allows to respect the DERs' current capabilities at all times, regardless of the dynamic changes occurring in the MG.

The non-ideal MG scenarios of having distorted voltages and non-steady voltage profiles are also discussed in this paper, validating through experimental results that the GCBC is resilient to operate under such conditions. Hence, proportional current sharing can also be supported for both scenarios, without causing overvoltages or overcurrents in the MG. The results show that the GCBC allows to obtain low-distortion currents at the MG PCC by the sharing of harmonic components by the DERs, even under distorted voltages. Moreover, voltage sags and swells are tested, indicating that the LVRT and HVRT capabilities of the GCBC strategy are satisfactory for MG perspectives.

Future works intend to experimentally assess the implementation of the GCBC in three-phase LV MGs, considering additional operational challenges. For instance, the condition of having asymmetrical voltages in the MG is one of the targeted possibilities for the next studies. Moreover, the concomitant existence of DERs from different hardware topologies, such as single-phase and three-phase inverters, is being studied to understand the pros and cons of implementing the GCBC approach.

Author Contributions: Conceptualization: A.M.S.A., D.I.B., E.T. and F.P.M.; methodology: A.M.S.A., D.I.B., E.T. and F.P.M.; validation: A.M.S.A. and L.D.O.A.; writing, review and editing: A.M.S.A., L.D.O.A., D.I.B., E.T., R.Q.M. and F.P.M.; funding acquisition: E.T. and F.P.M. All authors have read and agreed to the published version of the manuscript.

Funding: The authors are grateful to the São Paulo Research Foundation (FAPESP) (Grants 2019/22304-8, 2017/24652-8 and 2016/08645-9) and the Research Council of Norway (Grant f261735/H30).

Institutional Review Board Statement: Not applicable.

Informed Consent Statement: Not applicable.

Data Availability Statement: Not applicable.

Acknowledgments: The authors thank the São Paulo State University (UNESP) for providing financial support for the publication of this research.

Conflicts of Interest: The authors declare no conflict of interest. The funders had no role in the design of the study; in the collection, analyses, or interpretation of data; in the writing of the manuscript; or in the decision to publish the results.

Abbreviations

The following abbreviations are used in this manuscript:

AC	Alternating Current
DC	Direct Current
DER	Distributed Energy Resource
d-DER	Dispatchable DER
GCBC	Generalized Current-Based Control
MG	Microgrid
MGCC	Microgrid Central Controller
nd-DER	Non-dispatchable DER
PCC	MG Point of Common Coupling
PoC	Point of Connection of a DER

References

1. Li, S.; Lian, J.; Conejo, A.J.; Zhang, W. Transactive Energy Systems: The Market-Based Coordination of Distributed Energy Resources. *IEEE Control. Syst. Mag.* **2020**, *40*, 26–52. [\[CrossRef\]](#)
2. Eid, C.; Codani, P.; Perez, Y.; Reneses, J.; Hakvoort, R. Managing electric flexibility from Distributed Energy Resources: A review of incentives for market design. *Renew. Sustain. Energy Rev.* **2016**, *64*, 237–247. [\[CrossRef\]](#)
3. Hashemi, S.; Østergaard, J. Efficient Control of Energy Storage for Increasing the PV Hosting Capacity of LV Grids. *IEEE Trans. Smart Grid* **2018**, *9*, 2295–2303. [\[CrossRef\]](#)
4. Kumar, G.V.B.; Palanisamy, K. A Review of Energy Storage Participation for Ancillary Services in a Microgrid Environment. *Energies* **2020**, *5*, 63. [\[CrossRef\]](#)
5. Yang, Y.; Blaabjerg, F.; Wang, H.; Simoes, M.G. Power control flexibilities for grid-connected multi-functional photovoltaic inverters. *IET Renew. Power Gener.* **2016**, *10*, 504–513. [\[CrossRef\]](#)
6. Mirafzal, B.; Adib, A. On Grid-Interactive Smart Inverters: Features and Advancements. *IEEE Access* **2020**, *8*, 160526–160536. [\[CrossRef\]](#)
7. Arbab-Zavar, B.; Palacios-Garcia, E.J.; Vasquez, J.C.; Guerrero, J.M. Smart Inverters for Microgrid Applications: A Review. *Energies* **2019**, *12*, 840. [\[CrossRef\]](#)
8. Xue, Y.; Starke, M.; Dong, J.; Olama, M.; Kuruganti, T.; Taft, J.; Shankar, M. On a Future for Smart Inverters with Integrated System Functions. In Proceedings of the 2018 9th IEEE International Symposium on Power Electronics for Distributed Generation Systems (PEDG), Charlotte, NC, USA, 25–28 June 2018; pp. 1–8. [\[CrossRef\]](#)
9. Hu, J.; Shan, Y.; Cheng, K.W.; Islam, S. Overview of Power Converter Control in Microgrids: Challenges, Advances, and Future Trends. *IEEE Trans. Power Electron.* **2022**, *37*, 9907–9922. [\[CrossRef\]](#)
10. IEEE. IEEE Standard for the Specification of Microgrid Controllers. *IEEE Std.* **2018**, *1*, 1–43.
11. Aybar-Mejia, M.; Villanueva, J.; Mariano-Hernández, D.; Santos, F.; Molina-García, A. A Review of Low-Voltage Renewable Microgrids: Generation Forecasting and Demand-Side Management Strategies. *Electronics* **2021**, *10*, 2093. [\[CrossRef\]](#)
12. Guerrero, J.M.; Vasquez, J.C.; Matas, J.; de Vicuna, L.G.; Castilla, M. Hierarchical Control of Droop-Controlled AC and DC Microgrids—A General Approach Toward Standardization. *IEEE Trans. Ind. Electron.* **2011**, *58*, 158–172. [\[CrossRef\]](#)
13. Carpintero-Rentería, M.; Santos-Martín, D.; Guerrero, J.M. Microgrids Literature Review through a Layers Structure. *Energies* **2019**, *12*, 4381. [\[CrossRef\]](#)
14. Olivares, D.E.; Mehrizi-Sani, A.; Etemadi, A.H.; Cañizares, C.A.; Iravani, R.; Kazerani, M.; Hajimiragha, A.H.; Gomis-Bellmunt, O.; Saeedifard, M.; Palma-Behnke, R.; et al. Trends in Microgrid Control. *IEEE Trans. Smart Grid* **2014**, *5*, 1905–1919. [\[CrossRef\]](#)
15. Lasseter, R.H. Smart Distribution: Coupled Microgrids. *Proc. IEEE* **2011**, *99*, 1074–1082. [\[CrossRef\]](#)
16. Li, Z.; Shahidehpour, M.; Aminifar, F.; Alabdulwahab, A.; Al-Turki, Y. Networked Microgrids for Enhancing the Power System Resilience. *Proc. IEEE* **2017**, *105*, 1289–1310. [\[CrossRef\]](#)
17. Abedini, H.; Caldognetto, T.; Mattavelli, P.; Tenti, P. Real-Time Validation of Power Flow Control Method for Enhanced Operation of Microgrids. *Energies* **2020**, *13*, 5959. [\[CrossRef\]](#)
18. Junior, J.R.S.; Brandao, D.I.; Fernandes, N.T.D.; Utuerbey, W.; Cardoso, B. Multifunctional dispatchable microgrids. *Appl. Energy* **2021**, *282*, 116165. [\[CrossRef\]](#)
19. Hirsch, A.; Parag, Y.; Guerrero, J.M. Microgrids: A review of technologies, key drivers, and outstanding issues. *Renew. Sustain. Energy Rev.* **2018**, *90*, 402–411. [\[CrossRef\]](#)
20. De Araujo, L.S.; Alonso, A.M.S.; Brandao, D.I. Decentralized Control of Voltage- and Current-Controlled Converters Based on AC Bus Signaling for Autonomous Microgrids. *IEEE Access* **2020**, *8*, 202075–202089. [\[CrossRef\]](#)
21. Saleh, M.; Esa, Y.; Hariri, M.E.; Mohamed, A. Impact of Information and Communication Technology Limitations on Microgrid Operation. *Energies* **2019**, *12*, 2926. [\[CrossRef\]](#)
22. Micallef, A. Review of the current challenges and methods to mitigate power quality issues in single-phase microgrids. *IET Gener. Transm. Distrib.* **2019**, *13*, 2044–2054. [\[CrossRef\]](#)
23. Vijay, A.S.; Doolla, S.; Chandorkar, M.C. Unbalance mitigation strategies in microgrids. *IET Power Electron.* **2020**, *13*, 1687–1710. [\[CrossRef\]](#)
24. Micallef, A.; Apap, M.; Spiteri-Staines, C.; Guerrero, J.M.; Vasquez, J.C. Reactive Power Sharing and Voltage Harmonic Distortion Compensation of Droop Controlled Single Phase Islanded Microgrids. *IEEE Trans. Smart Grid* **2014**, *5*, 1149–1158. [\[CrossRef\]](#)
25. Vasquez, J.C.; Mastromauro, R.A.; Guerrero, J.M.; Liserre, M. Voltage Support Provided by a Droop-Controlled Multifunctional Inverter. *IEEE Trans. Ind. Electron.* **2009**, *56*, 4510–4519. [\[CrossRef\]](#)
26. Yazdavar, A.H.; Azzouz, M.A.; El-Saadany, E.F. A Novel Decentralized Control Scheme for Enhanced Nonlinear Load Sharing and Power Quality in Islanded Microgrids. *IEEE Trans. Smart Grid* **2019**, *10*, 29–39. [\[CrossRef\]](#)
27. Afshar, Z.; Mollayousefi, M.; Bathaee, S.M.T.; Bina, M.T.; Gharehpetian, G.B. A Novel Accurate Power Sharing Method Versus Droop Control In Autonomous Microgrids With Critical Loads. *IEEE Access* **2019**, *7*, 89466–89474. [\[CrossRef\]](#)
28. Sreekumar, P.; Khadkikar, V. Direct Control of the Inverter Impedance to Achieve Controllable Harmonic Sharing in the Islanded Microgrid. *IEEE Trans. Ind. Electron.* **2017**, *64*, 827–837. [\[CrossRef\]](#)
29. Deng, W.; Dai, N.; Lao, K.W.; Guerrero, J.M. A Virtual-Impedance Droop Control for Accurate Active Power Control and Reactive Power Sharing Using Capacitive-Coupling Inverters. *IEEE Trans. Ind. Appl.* **2020**, *56*, 6722–6733. [\[CrossRef\]](#)

30. Wu, D.; Tang, F.; Dragicevic, T.; Vasquez, J.C.; Guerrero, J.M. Autonomous Active Power Control for Islanded AC Microgrids With Photovoltaic Generation and Energy Storage System. *IEEE Trans. Energy Convers.* **2014**, *29*, 882–892. [[CrossRef](#)]
31. Han, H.; Hou, X.; Yang, J.; Wu, J.; Su, M.; Guerrero, J.M. Review of Power Sharing Control Strategies for Islanding Operation of AC Microgrids. *IEEE Trans. Smart Grid* **2016**, *7*, 200–215. [[CrossRef](#)]
32. Avila, L.I.; Castanon, L.E.; Martinez, A.V.; Zhang, Y. A Review of Optimal Control Techniques Applied to the Energy Management and Control of Microgrids. *Procedia Comput. Sci.* **2015**, *52*, 780–787. [[CrossRef](#)]
33. Soshinskaya, M.; Crijns-Graus, W.H.; Guerrero, J.M.; Vasquez, J.C. Microgrids: Experiences, barriers and success factors. *Renew. Sustain. Energy Rev.* **2014**, *40*, 659–672. [[CrossRef](#)]
34. Cheng, Z.; Duan, J.; Chow, M. To Centralize or to Distribute: That Is the Question: A Comparison of Advanced Microgrid Management Systems. *IEEE Ind. Electron. Mag.* **2018**, *12*, 6–24. [[CrossRef](#)]
35. Caldognetto, T.; Tenti, P.; Costabeber, A.; Mattavelli, P. Improving Microgrid Performance by Cooperative Control of Distributed Energy Sources. *IEEE Trans. Ind. Appl.* **2014**, *50*, 3921–3930. [[CrossRef](#)]
36. Cavraro, G.; Caldognetto, T.; Carli, R.; Tenti, P. A Master/Slave Approach to Power Flow and Overvoltage Control in Low-Voltage Microgrids. *Energies* **2019**, *12*, 2760. [[CrossRef](#)]
37. Morales-Paredes, H.K.; Bonaldo, J.P.; Pomilio, J.A. Centralized Control Center Implementation for Synergistic Operation of Distributed Multifunctional Single-Phase Grid-Tie Inverters in a Microgrid. *IEEE Trans. Ind. Electron.* **2018**, *65*, 8018–8029. [[CrossRef](#)]
38. Caldognetto, T.; Buso, S.; Tenti, P.; Brandao, D.I. Power-Based Control of Low-Voltage Microgrids. *IEEE J. Emerg. Sel. Top. Power Electron.* **2015**, *3*, 1056–1066. [[CrossRef](#)]
39. Zeng, Z.; Zhao, R.; Yang, H. Coordinated control of multi-functional grid-tied inverters using conductance and susceptance limitation. *IET Power Electron.* **2014**, *7*, 1821–1831. [[CrossRef](#)]
40. Dos, Reis, G.; Liberado, E.; Marafão, F.; Sousa, C.; Silva, W.; Brandao, D. Model-Free Power Control for Low-Voltage AC Dispatchable Microgrids with Multiple Points of Connection. *Energies* **2021**, *14*, 6390. [[CrossRef](#)]
41. Zhao, Y.; Yu, J.; Ban, M.; Liu, Y.; Li, Z. Privacy-Preserving Economic Dispatch for An Active Distribution Network With Multiple Networked Microgrids. *IEEE Access* **2018**, *6*, 38802–38819. [[CrossRef](#)]
42. Tenti, P.; Caldognetto, T. On Microgrid Evolution to Local Area Energy Network (E-LAN). *IEEE Trans. Smart Grid* **2019**, *10*, 1567–1576. [[CrossRef](#)]
43. Alonso, A.M.S.; Brandao, D.I.; Caldognetto, T.; Marafao, F.P.; Mattavelli, P. A selective harmonic compensation and power control approach exploiting distributed electronic converters in microgrids. *Int. J. Electr. Power Energy Syst.* **2020**, *115*, 1–15. [[CrossRef](#)]
44. Alonso, A.M.S.; Brandao, D.I.; Tedeschi, E.; Marafão, F.P. Distributed selective harmonic mitigation and decoupled unbalance compensation by coordinated inverters in three-phase four-wire low-voltage networks. *Electr. Power Syst. Res.* **2020**, *186*, 106407. [[CrossRef](#)]
45. Alonso, A.M.S.; Göthner, F.; Brandao, D.I.; Marafao, F.P.; Tedeschi, E. Power- and Current-Based Control of Distributed Inverters in Low-Voltage Microgrids: Considerations in Relation to Classic Droop Control. In Proceedings of the 2020 Fifteenth International Conference on Ecological Vehicles and Renewable Energies (EVER), Monte-Carlo, Monaco, 10–12 September 2020; pp. 1–10. [[CrossRef](#)]
46. Rocabert, J.; Luna, A.; Blaabjerg, F.; Rodríguez, P. Control of Power Converters in AC Microgrids. *IEEE Trans. Power Electron.* **2012**, *27*, 4734–4749. [[CrossRef](#)]
47. IEEE. IEEE Standard for Interconnection and Interoperability of Distributed Energy Resources with Asiated Electric Power Systems Interfaces. *IEEE Stand.* **2018**, *1*, 1–138. [[CrossRef](#)]
48. Han, Y.; Li, H.; Shen, P.; Coelho, E.A.A.; Guerrero, J.M. Review of Active and Reactive Power Sharing Strategies in Hierarchical Controlled Microgrids. *IEEE Trans. Power Electron.* **2017**, *32*, 2427–2451. [[CrossRef](#)]
49. Ziouani, I.; Boukhetala, D.; Darcherif, A.M.; Amghar, B.; El Abbassi, I. Hierarchical control for flexible microgrid based on three-phase voltage source inverters operated in parallel. *Int. J. Electr. Power Energy Syst.* **2018**, *95*, 188–201. [[CrossRef](#)]
50. Zia, M.F.; Benbouzid, M.; Elbouchikhi, E.; Muyeen, S.M.; Techato, K.; Guerrero, J.M. Microgrid Transactive Energy: Review, Architectures, Distributed Ledger Technologies, and Market Analysis. *IEEE Access* **2020**, *8*, 19410–19432. [[CrossRef](#)]
51. Padua, M.S.; Deckmann, S.M.; Marafao, F.P. Frequency-Adjustable Positive Sequence Detector for Power Conditioning Applications. In Proceedings of the 2005 IEEE 36th Power Electronics Specialists Conference, Dresden, Germany, 16 June 2005; pp. 1928–1934. [[CrossRef](#)]
52. Oppenheim, A.V.; Schaffer, R.W. *Discrete-Time Signal Processing*, 3rd ed.; Prentice Hall Press: Upper Saddle River, NJ, USA, 2009.
53. Park, S.; Han, S.B.; Jung, B.M.; Choi, S.H.; Jeong, H.G. A current control scheme based on multiple synchronous reference frames for parallel hybrid active filter. In Proceedings of the IP EMC 2000. Third International Power Electronics and Motion Control Conference (IEEE Cat. No. 00EX435), Beijing, China, 15–18 August 2000; Volume 1, pp. 218–223. [[CrossRef](#)]
54. Xavier, L.S.; Cupertino, A.F.; de Resende, J.T.; Mendes, V.F.; Pereira, H.A. Adaptive current control strategy for harmonic compensation in single-phase solar inverters. *Electr. Power Syst. Res.* **2017**, *142*, 84–95. [[CrossRef](#)]
55. Xu, Q.; Xiao, J.; Hu, X.; Wang, P.; Lee, M.Y. A Decentralized Power Management Strategy for Hybrid Energy Storage System With Autonomous Bus Voltage Restoration and State-of-Charge Recovery. *IEEE Trans. Ind. Electron.* **2017**, *64*, 7098–7108. [[CrossRef](#)]
56. SMA. The Self-Consumption Bonus: Information and Details Regarding The Self-Consumption of Solar Energy. Available online: <https://www.sma.de/en/partners/knowledgebase/the-self-consumption-bonus.html> (accessed on 29 December 2020).

57. Martins, M.A.I.; Fernandes, R.; Heldwein, M.L. Proposals for Regulatory Framework Modifications for Microgrid Insertion—The Brazil Use Case. *IEEE Access* **2020**, *8*, 94852–94870. [[CrossRef](#)]
58. Alonso, A.M.S.; Brandao, D.I.; Marafão, F.P.; Tedeschi, E. Coordinated Control of Parallel Power Conditioners Synthesizing Resistive Loads in Single-Phase AC Microgrids. In Proceedings of the 2019 21st European Conference on Power Electronics and Applications (EPE '19 ECCE Europe), Genova, Italy, 3–5 September 2019; pp. 1–9. [[CrossRef](#)]
59. Liberado, E.V.; Pomilio, J.A.; Alonso, A.M.S.; Tedeschi, E.; Marafão, F.P.; Guerreiro, J.F. Three/Four-leg Inverter Current Control Based on Generalized Symmetrical Components. In Proceedings of the 2018 IEEE 19th Workshop on Control and Modeling for Power Electronics (COMPEL), Padua, Italy, 25–28 June 2018; pp. 1–7. [[CrossRef](#)]
60. Alonso, A.M.S.; De Oro Arenas, L.; Hock, R.T.; Guillard, H.; Liberado, E.V.; Paredes, H.K.M.; Gonçalves, F.A.S.; Marafao, F.P. Experimental Implementation of a Single-Phase Microgrid: A Flexible Resource for Research and Educational Activities. In Proceedings of the 2021 Brazilian Power Electronics Conference (COBEP), João Pessoa, Brazil, 7–10 November 2021; pp. 1–8. [[CrossRef](#)]
61. Buso, S.; Mattavelli, P. *Digital Control in Power Electronics*, 2nd ed.; Morgan & Claypool: San Rafael, CA, USA, 2015.
62. Tenti, P.; Mattavelli, P. A Time Domain Approach to Power Term Definitions under Non Sinusoidal Conditions. *L'Energia Elettr.* **2004**, *81*, 1–10.
63. Adib, A.; Mirafzal, B. Virtual Inductance for Stable Operation of Grid-Interactive Voltage Source Inverters. *IEEE Trans. Ind. Electron.* **2019**, *66*, 6002–6011. [[CrossRef](#)]
64. He, J.; Li, Y.W.; Wang, R.; Zhang, C. Analysis and Mitigation of Resonance Propagation in Grid-Connected and Islanding Microgrids. *IEEE Trans. Energy Convers.* **2015**, *30*, 70–81. [[CrossRef](#)]
65. Nunez-Zuniga, T.E.; Pomilio, J.A. Shunt active power filter synthesizing resistive loads. *IEEE Trans. Power Electron.* **2002**, *17*, 273–278. [[CrossRef](#)]
66. Marafao, F.P.; Brandao, D.I.; Costabeber, A.; Paredes, H.K.M. Multi-task control strategy for grid-tied inverters based on conservative power theory. *IET Renew. Power Gener.* **2015**, *9*, 154–165. [[CrossRef](#)]
67. Marafão, F.P.; dos Santos Alonso, A.M.; Gonçalves, F.A.S.; Brandão, D.I.; Martins, A.C.G.; Morales Paredes, H.K. Trends and Constraints on Brazilian Photovoltaic Industry: Energy Policies, Interconnection Codes, and Equipment Certification. *IEEE Trans. Ind. Appl.* **2018**, *54*, 4017–4027. [[CrossRef](#)]
68. Hiremath, R.; Moger, T. Comprehensive review on low voltage ride through capability of wind turbine generators. *Int. Trans. Electr. Energy Syst.* **2020**, *30*, e12524. [[CrossRef](#)]
69. Bottrell, N.; Green, T.C. Comparison of Current-Limiting Strategies During Fault Ride-Through of Inverters to Prevent Latch-Up and Wind-Up. *IEEE Trans. Power Electron.* **2014**, *29*, 3786–3797. [[CrossRef](#)]